the
abdus salam
international centre for theoretical physics

united nations
educational, scientific
and cultural
organization

international atomic
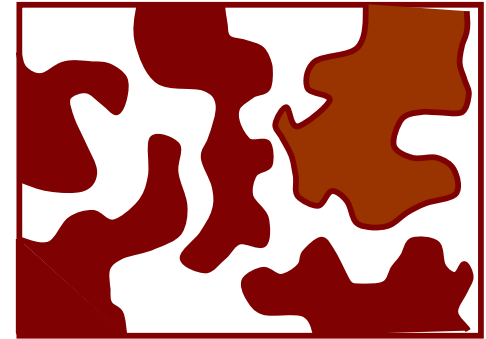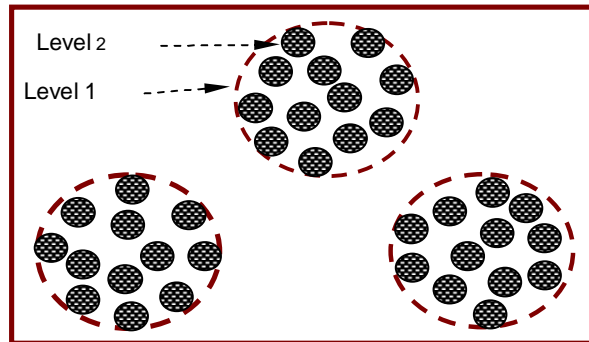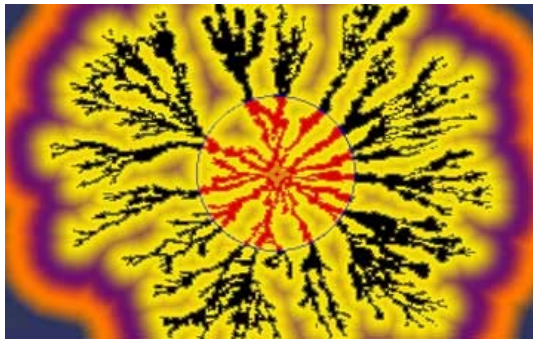energy agency

ICTP 40th Anniversary

1561/29

Nanophased materials concentrated systems
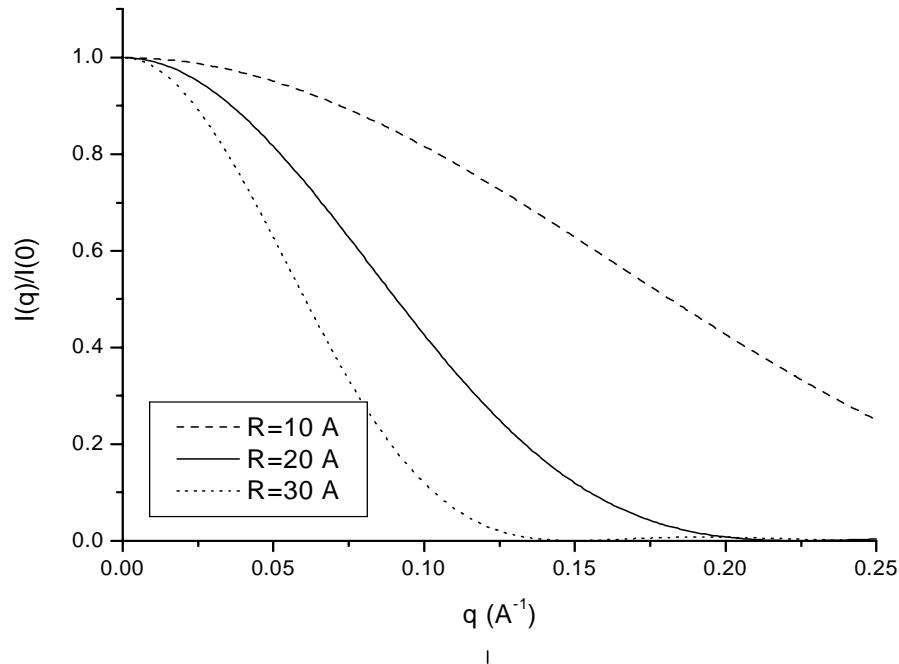
A. Craievich

Nanophased materials
Concentrated systems

Spherical nano-objects embedded in a homogeneous matrix

$$I(q) = N.I_1(q)$$

Monodisperse set of spheres

$$I_1(q) = I_e (\rho_1 - \rho_2)^2 . \left(\frac{4\pi R^3}{3} \right)^2 [\Phi(q)]^2$$

$$\Phi(q) = 3 \frac{\sin qR - qR \cos qR}{(qR)^3}$$

Intensity (a. u.)

q (A^{-1})

Legend:
- <R>=40 sig=0
- <R>=40sig=10
- <R>=40sig25
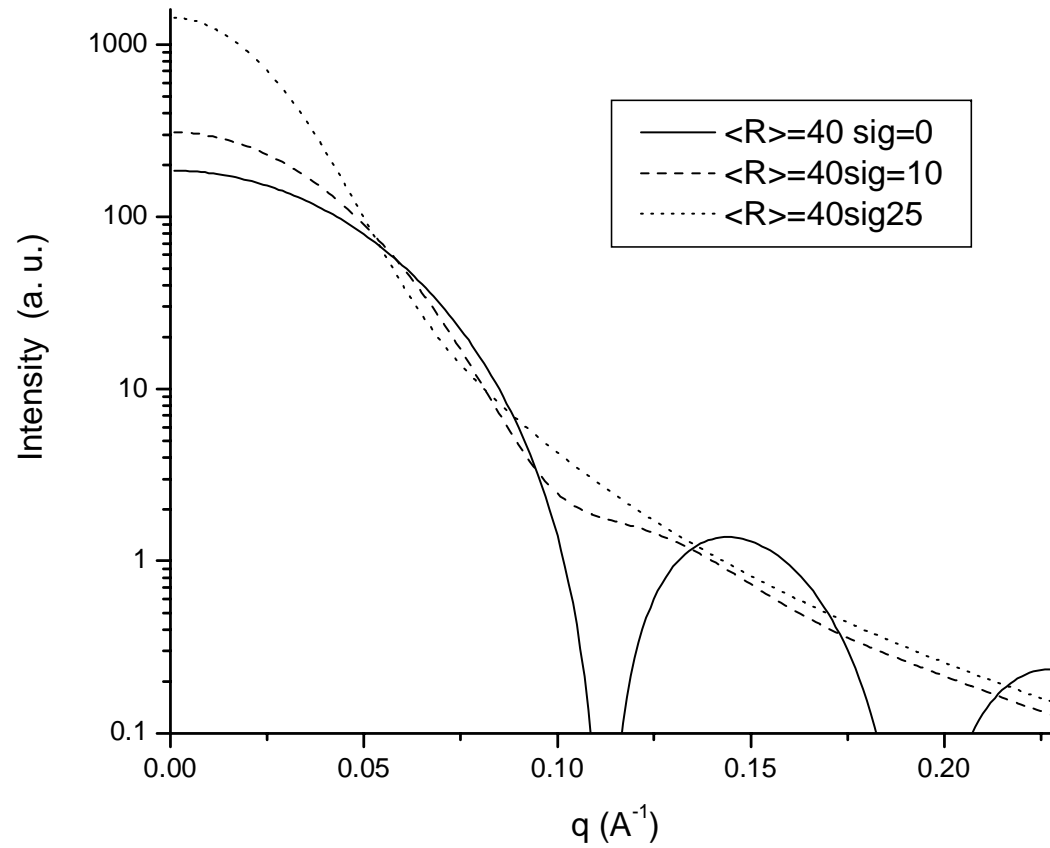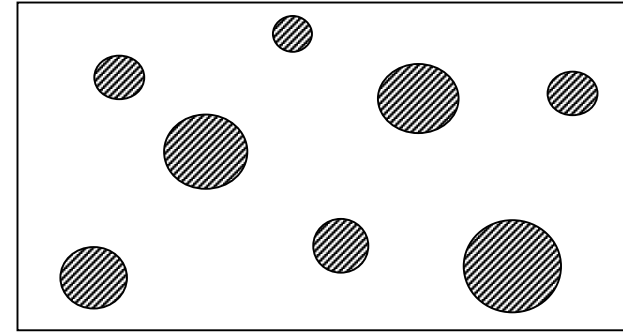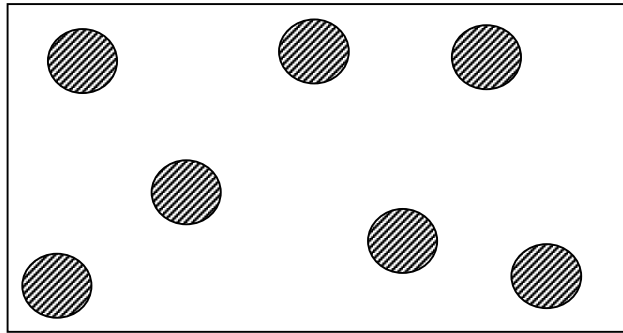
Same <R> and different dispersion

Process sol - gel
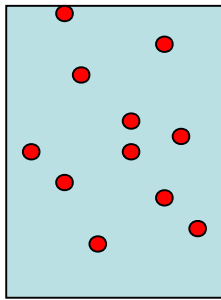
colloidal liquid sol   aggregation   sol-gel   aging   drying   sintering
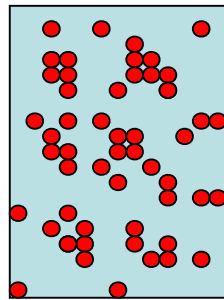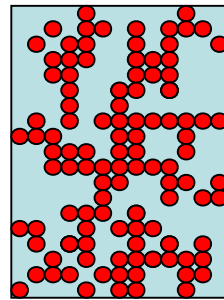
process   transition
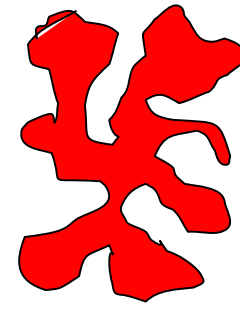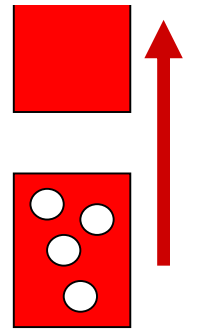
Fractal materials
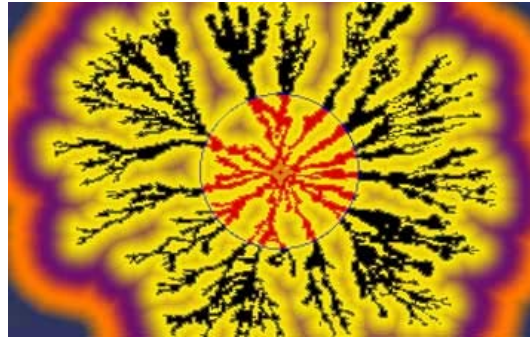
Structure characterization and mechanism of growth

50 Å

50 Å

50 Å
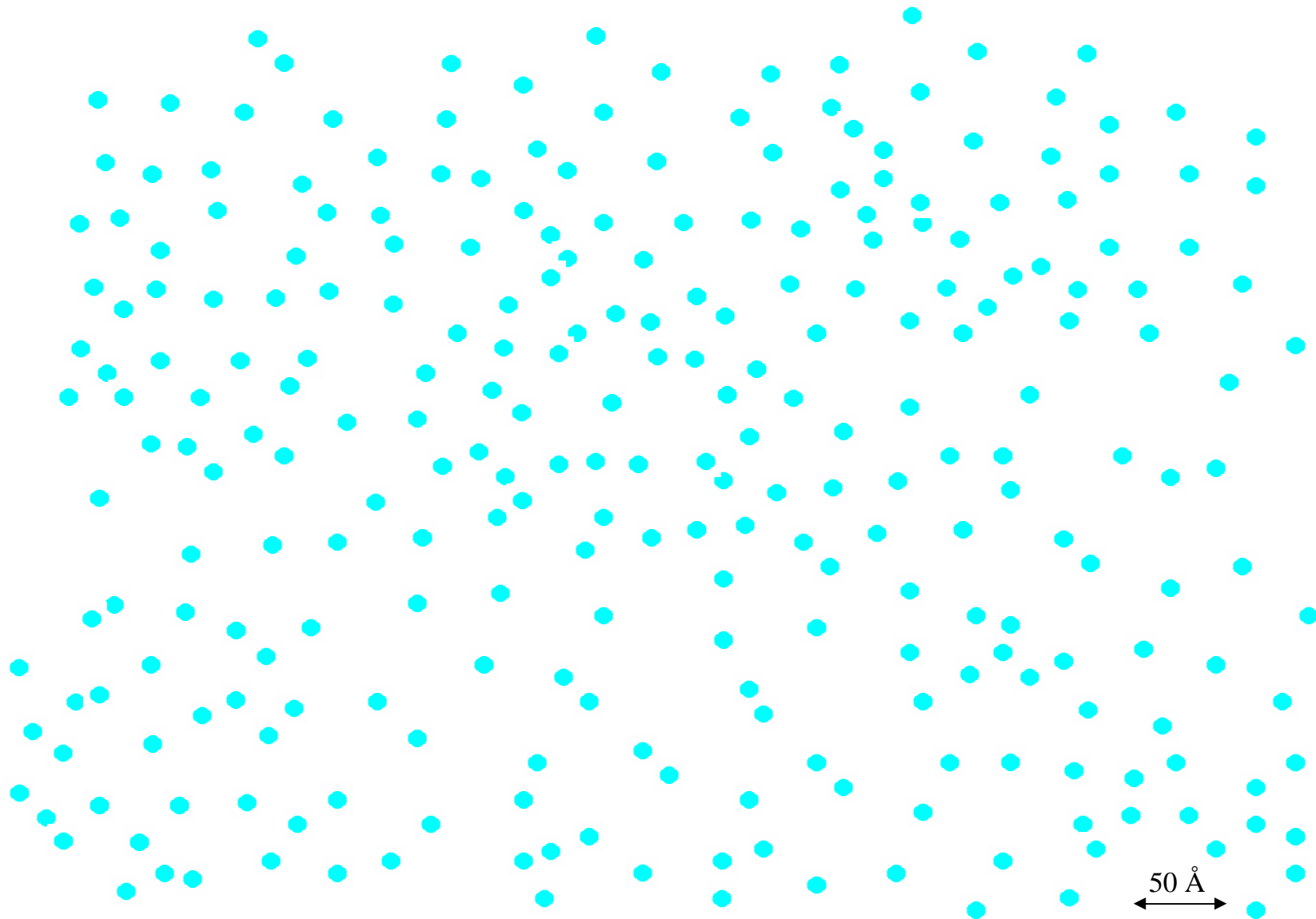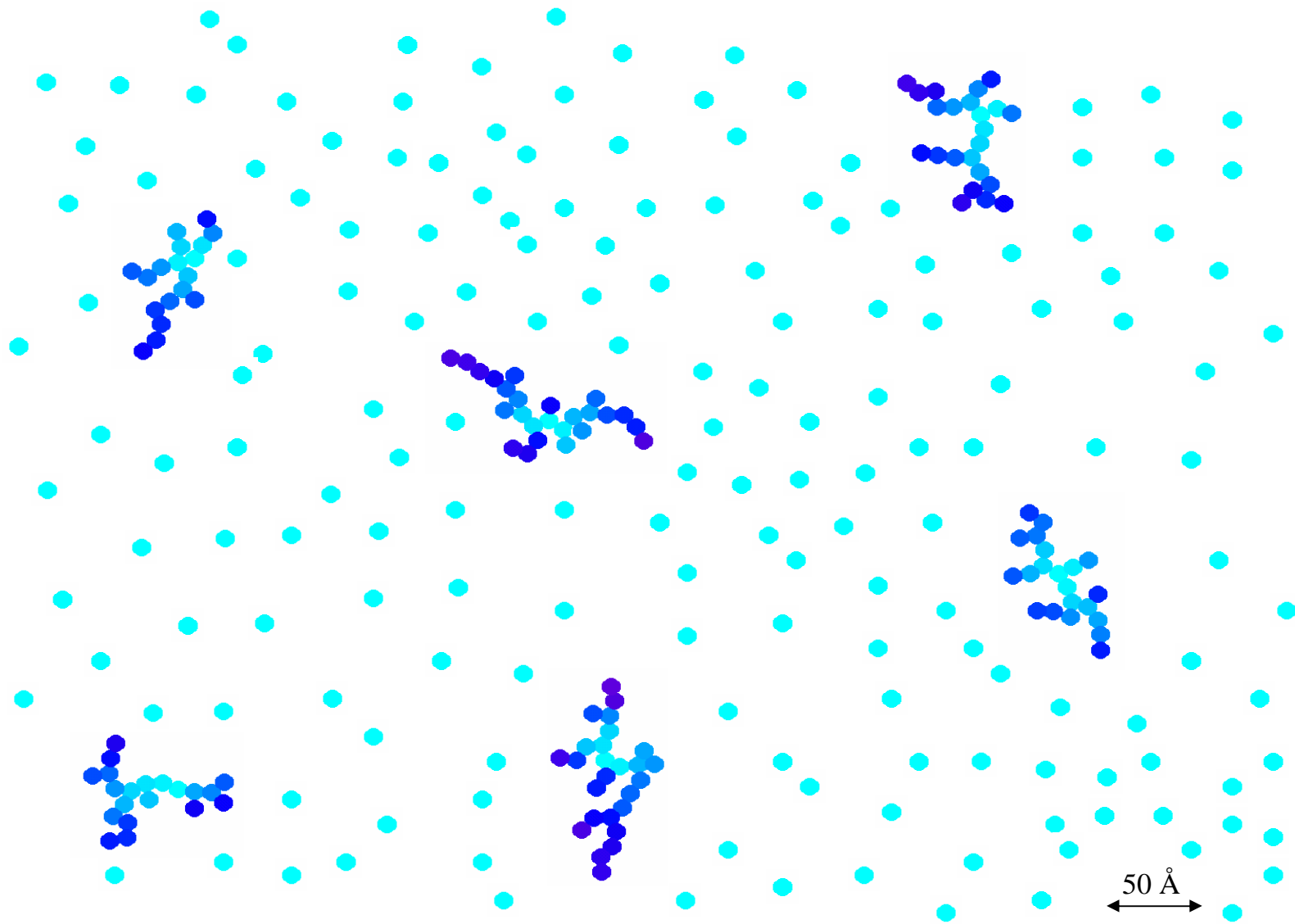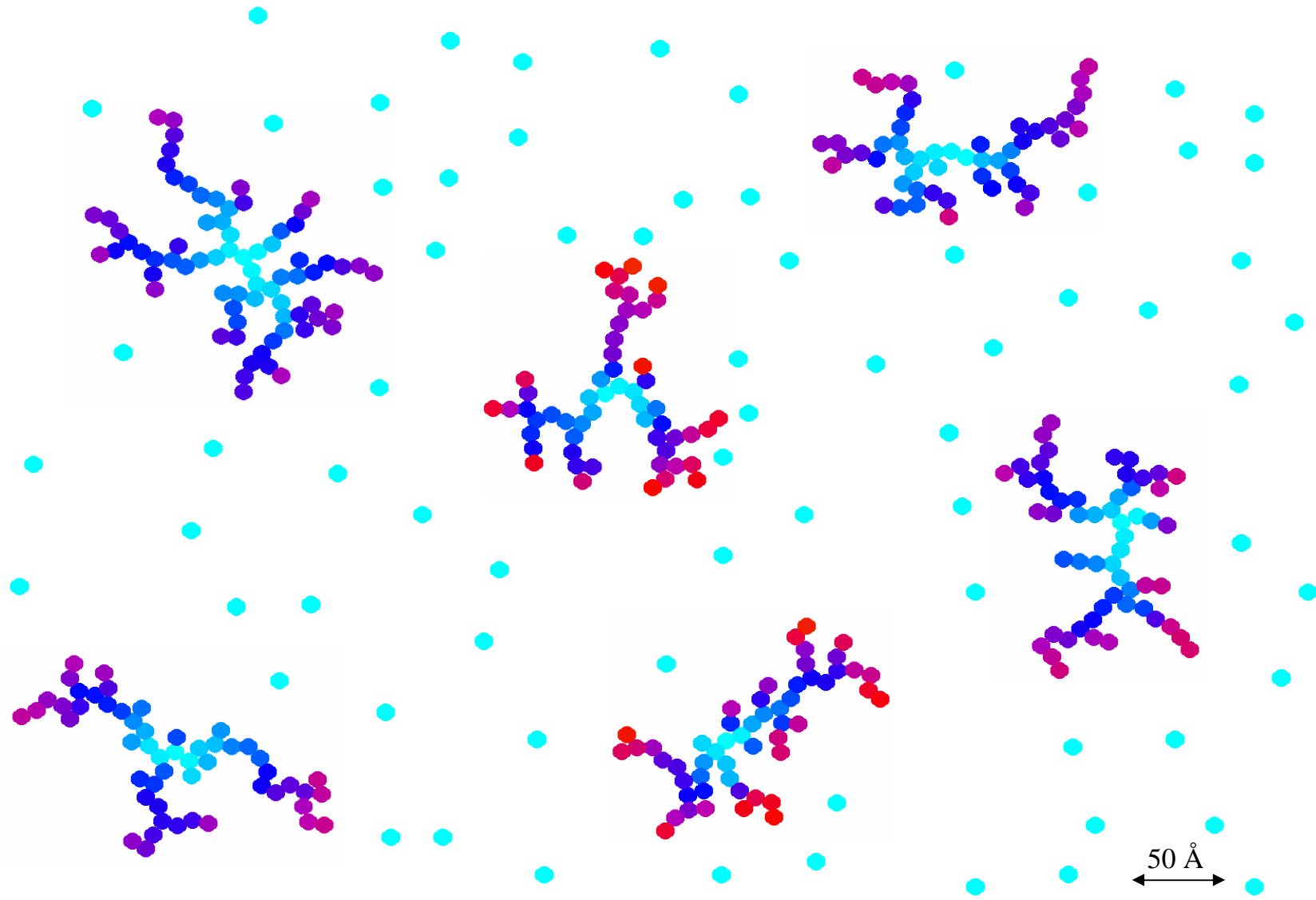
Fractal objects

$$\frac{M}{V} = \rho$$

$$M = \rho V = K r^3$$

$$\log M = A + 3 \log r$$

log M

tan α = 3

log R

log r

log M

tan α = 3

tan α = D
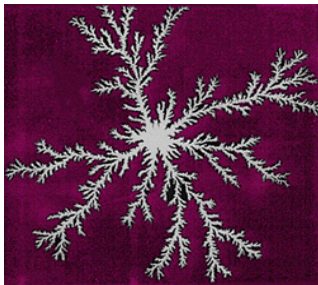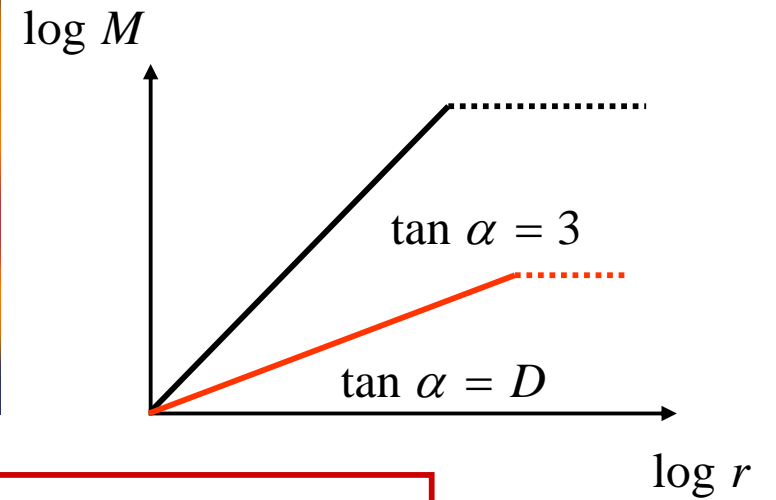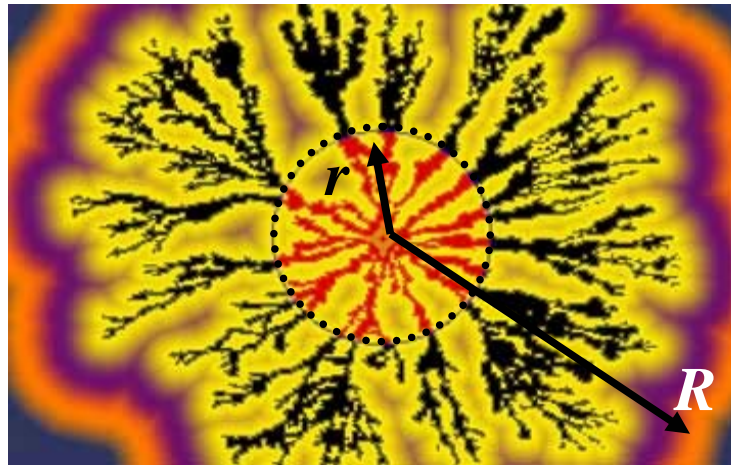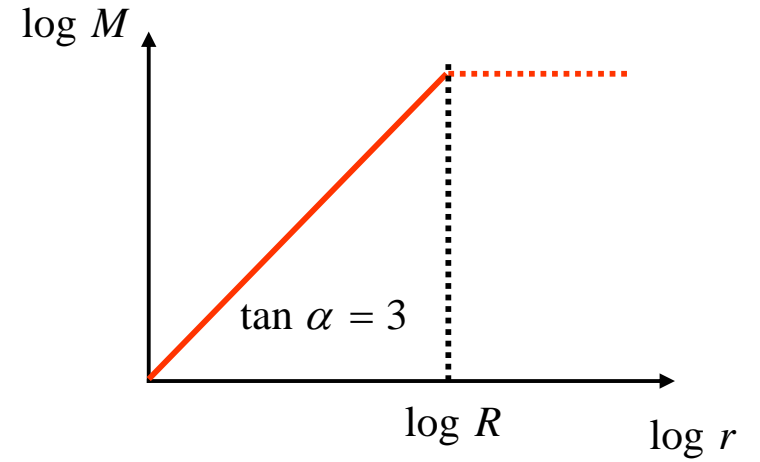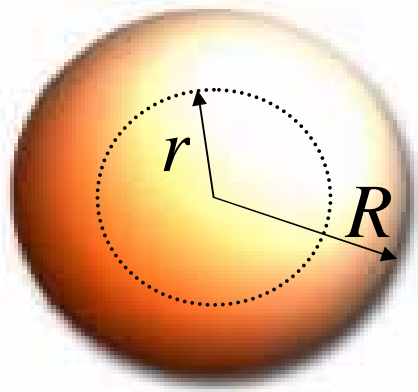
log r

$$M = K r^D$$

$$\log M = K + D \log r$$

Determination of the fractal dimension in real space
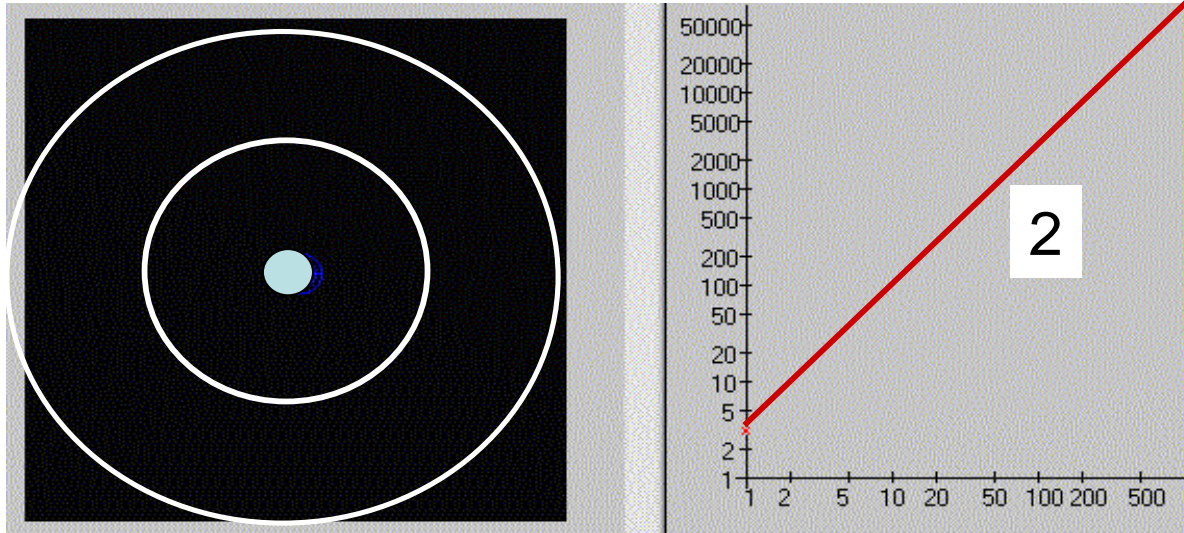
$M = k.R^2$

$Log\ M = a + 2.log\ R$
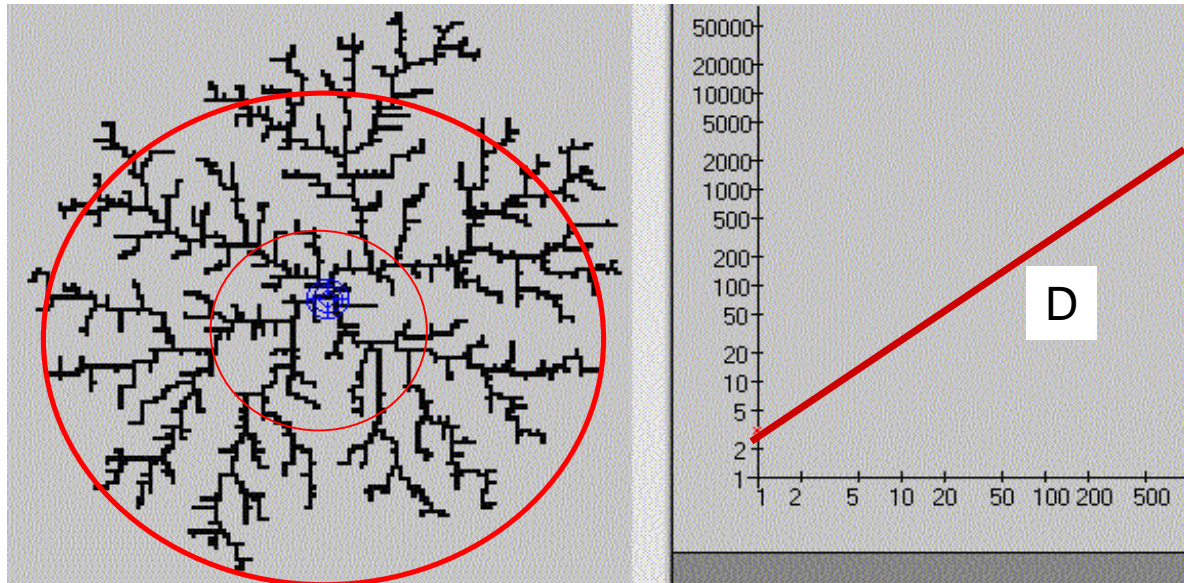
$M = k.R^D$

$Log\ M = a + D.log\ R$

$D < 2$

Aggregation of colloidal particles
Models of growth and results of calculations of the fractal dimension using computer simulation

Mechanism of growth	Fractal dimension (3D)	Fractal dimension (2D)
Eden		2
Witten Sanders	2.45	1.65-1.70
Witten Sanders linear trajectory	2.97	1.92-1.95
Tip-to-tip	1.43	1.26
Self-avoiding walk	1.66	1.33
Cluster-cluster random walk	1.75-1.80	1.44-1.48
Cluster-cluster ballistic	1.81-1.95	1.50-1.54
Ideal linear polymer	2.00	
Swollen linear polymer	1.66	
Ideal branched polymer	2.16	
Dense particle	3.00	
Diffusion limited cluster-cluster aggregation (DLCA)	1.78	
Reaction limited cluster-cluster aggregation (RLCA)	2.11	
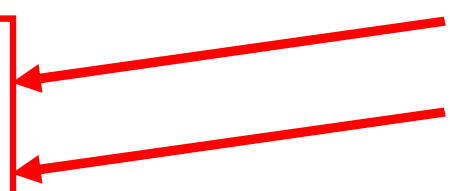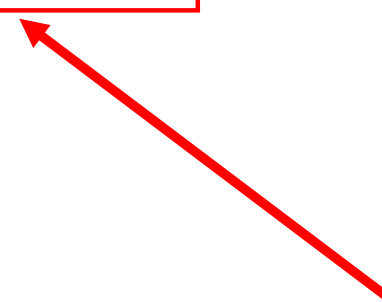
Concentrated set of centrosymmertical particles

$$I(q)=N.I_1(q). S(q)$$

Fractal systems

$$I_1(q) = \frac{A}{\left[1+(r_0 q)^2\right]^2}$$

$$S(q) = 1 + \frac{1}{\left(q r_0\right)^D} \frac{D.\Gamma(D-1)}{\left[1+1/(q^2 \xi^2)\right]^{(D-1)/2}} \sin\left[(D-1)\tan^{-1}(q\xi)\right]$$

$$R_g = \left[\frac{D(D+1)}{2}\right]^{1/2} \xi$$

Determination of the fractal dimension from SAXS curves

$$I(q) = \frac{A}{\left(1 + r_0^2 q^2\right)^2} \cdot \left\{ 1 + \frac{1}{\left(qr_0\right)^D} \frac{D.\Gamma(D-1)}{\left[1 + 1/(q^2\xi^2)\right]^{(D-1)/2}} \sin\left[(D-1)\tan^{-1}(q\xi)\right] \right\}$$

$$I(q) \propto q^{-D} \qquad (1/\xi << q << 1/r_0)$$

J. Teixeira   J. Appl. Cryst. 21, 781-785 (1988)

$$I(q) = N \cdot I_1(q) \cdot S(q)$$

$\xi = 10000 \text{ A}$ $D=1.8$ $R_0=10 \text{ A}$

Slope

Form factor (r_o=10 Å)
Structure factor
(**Fractal dimension = 1.8 and R = 10000 Å**
Scattering curve

Intensity (u.a.)

q (Å^{-1})
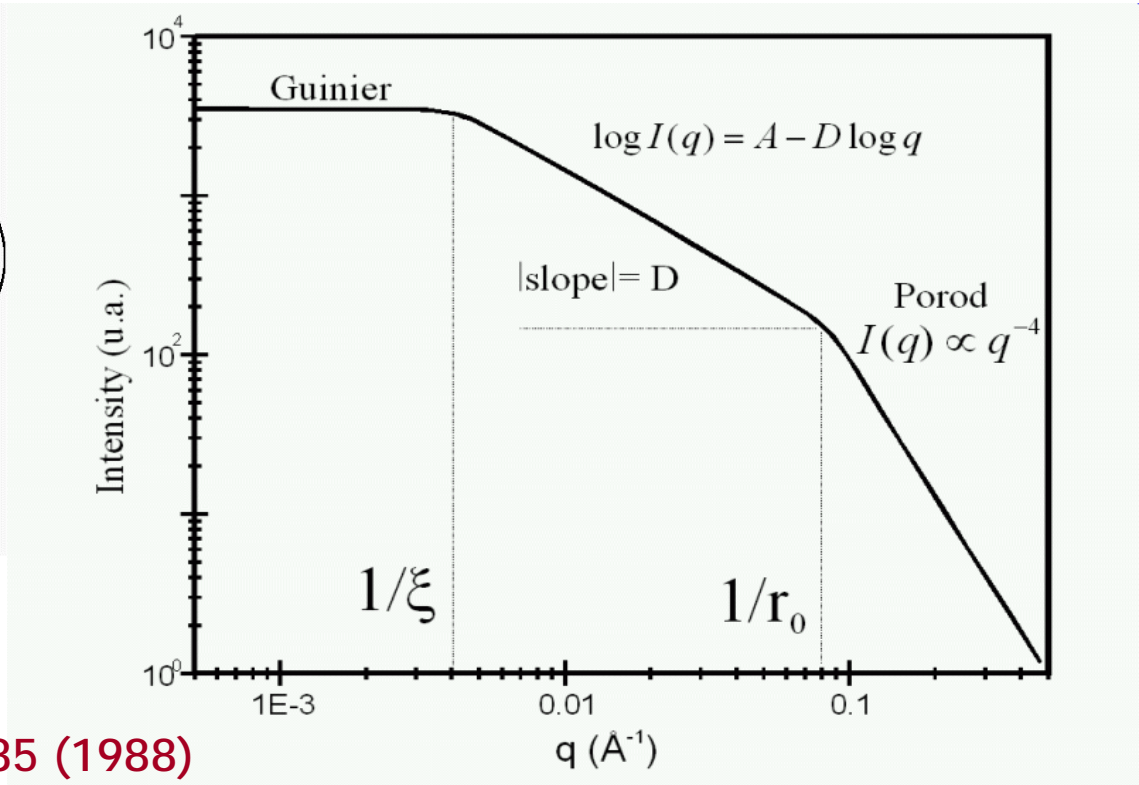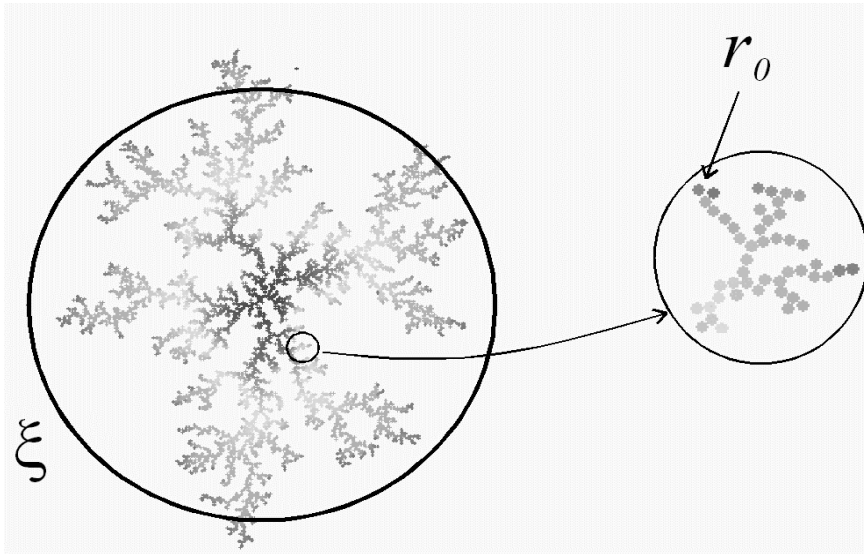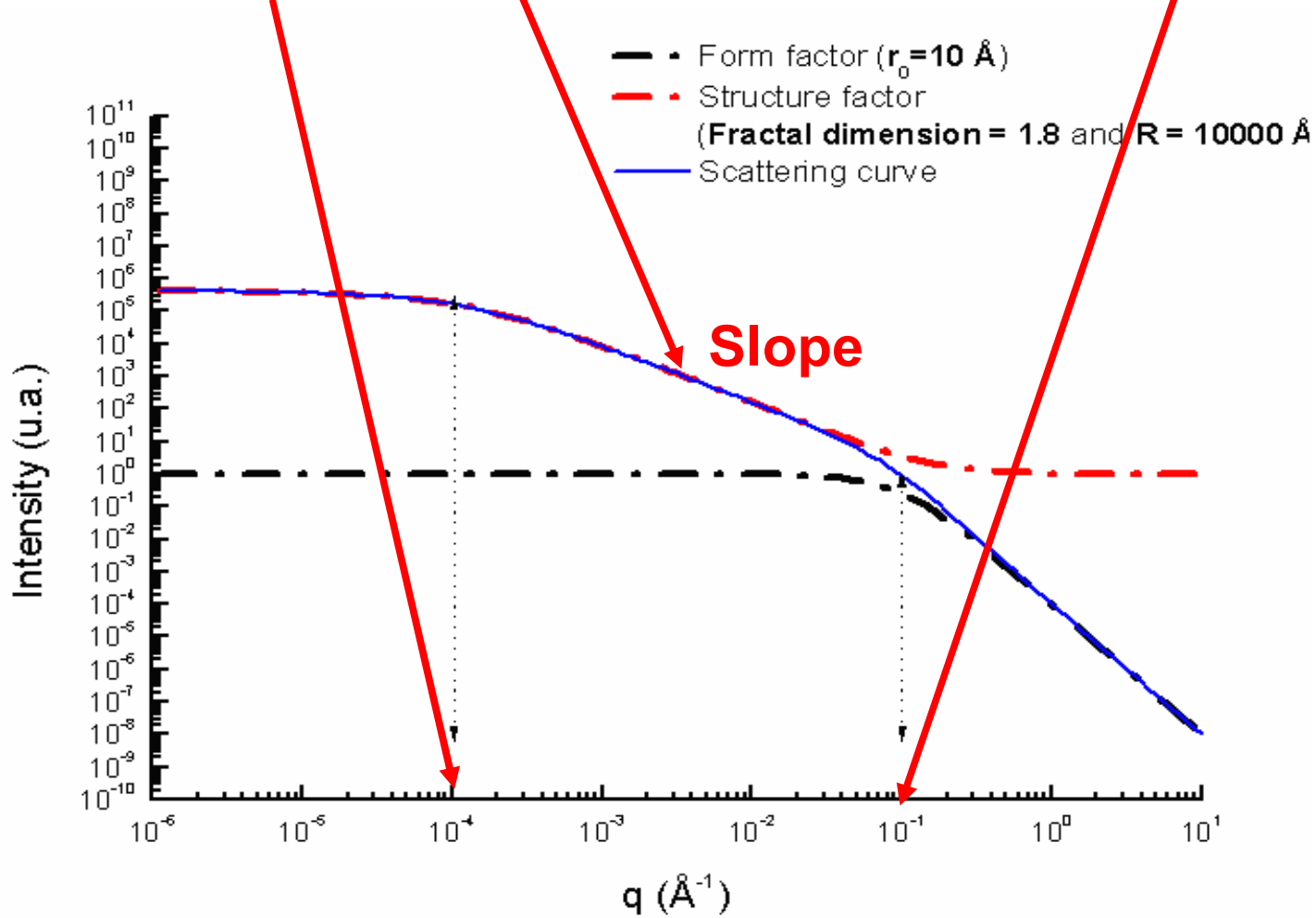
Fractal structure of basic silica gels with low Ca content
F. Gaboriaud, D. Chaumont, A. Nonat and A. Craievich
J. Appl. Cryst. 33, 597-9 (2000).

   The process leading to basic silica gels involves the formation of siloxane bond (Si-O-Si) induced by calcium ions. The formation of this gel is responsible for the degradation of concrete. The chemical process involved in the formation of these gels is called alkali-silica reaction (ASR). These gels have a fractal structure within an extremely large size scale (from 1 to 1000 nm).
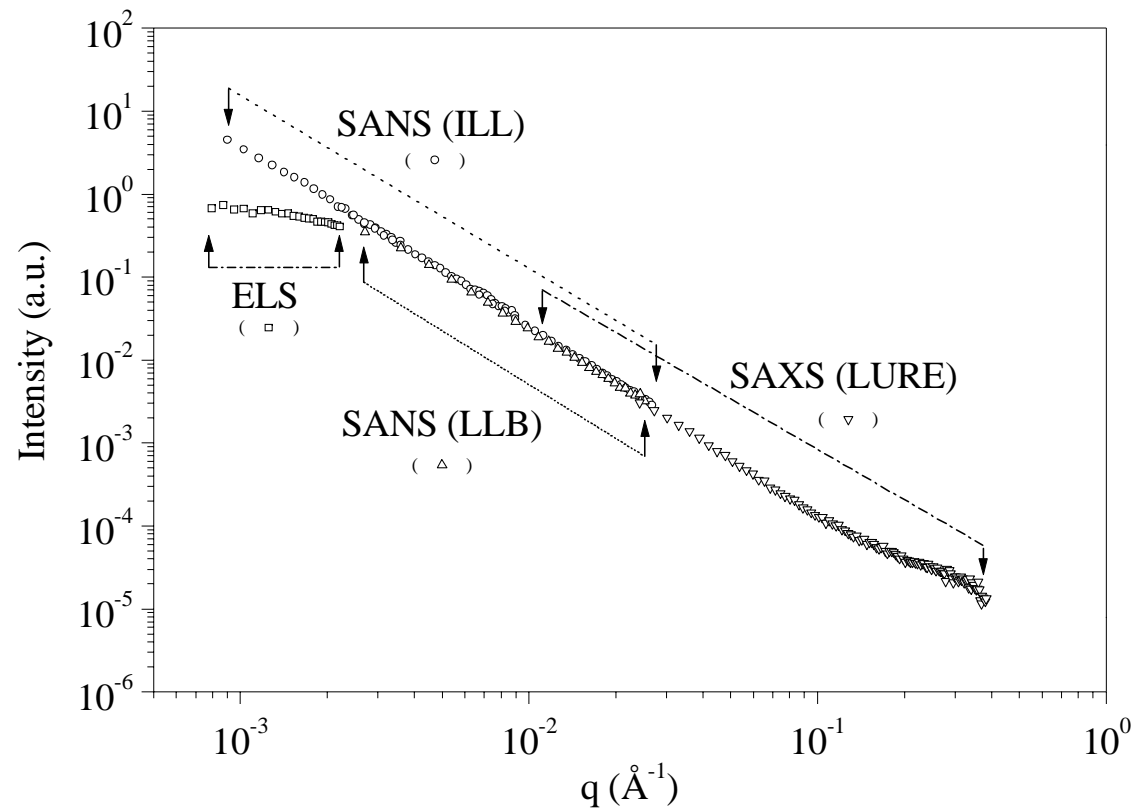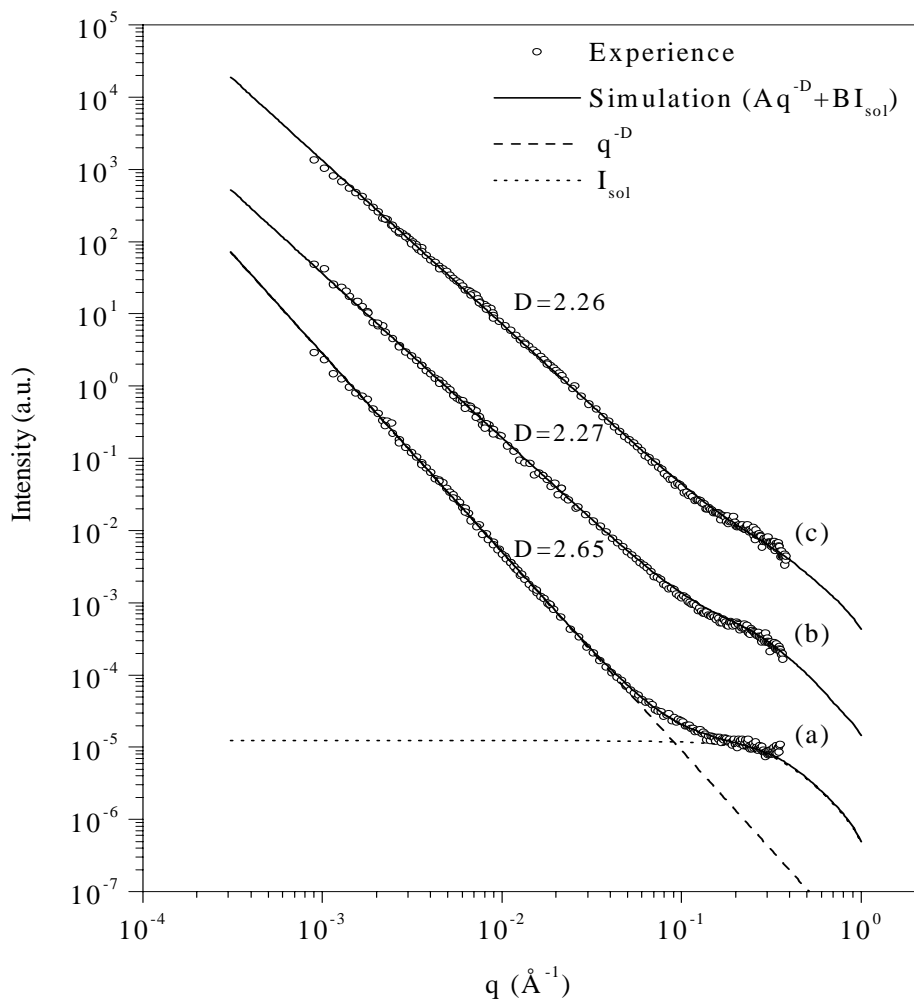
(b,c)
In these sample the fractal dimension is D=2.26 The aggregation predominantly occurs by reaction limited cluster-cluster aggregation (D_{the}=2.11)

(a)
The high fractal dimension (D=2.65) corresponds to a different mechanism of aggregation. An additional densification effect on the fractal aggregate, at high q, is produced by the progressive incorporation of primary particles remaining in the sol.

(a) $SiO_2/Na_2O=2$ + [$Ca(OH)_2$]=0.08mol.L^{-1} D=2.65
(b) $SiO_2/Na_2O=3$ + [$Ca(OH)_2$]=0.08mol.L^{-1} D=2.27
(c) $SiO_2/Li_2O=2$ + [$Ca(OH)_2$]=0.16mol.L^{-1} D=2.26
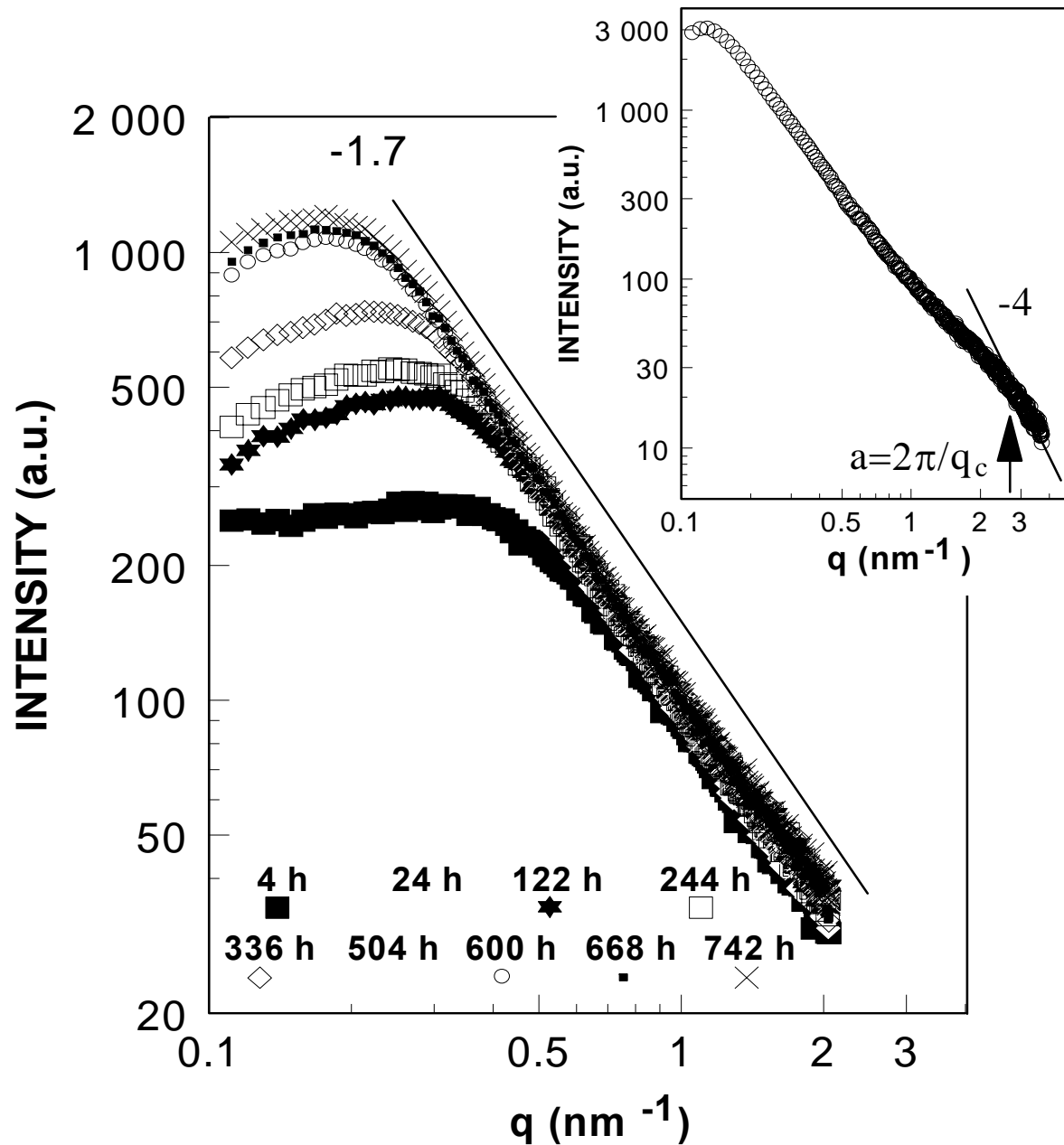
Zirconia-based sols. Log I vs. log q plots for increasing periods of time from 4 hours (bottom) up to 742 hours (top). The inset is the scattering intensity curve of the final gel obtained after a period of about twice the gelling time.

A. Lecomte, A. Dauger, P. Lenormand, J. Appl. Cryst. 33, 496-499 (2000).

In situ SAXS curves during the aggregation process

P. Riello, A. Minesso, A. Benedetti and A. Craievich, J. Phys. Chem. B 107, 3390 (2003)
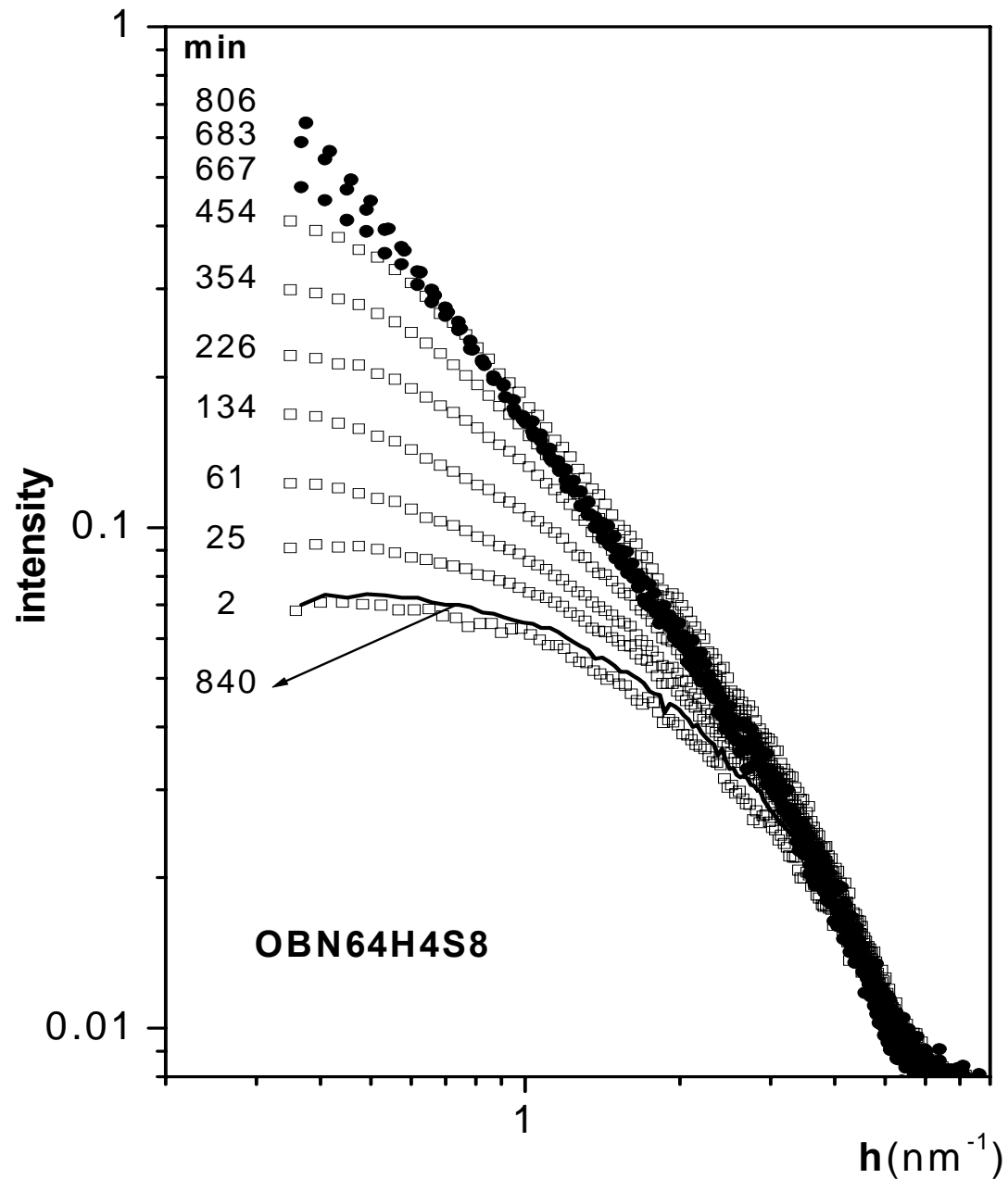
Fig.1

Modelling the SAXS curves assuming clusters of cilyndrical shape

Fig 12

Fig.7
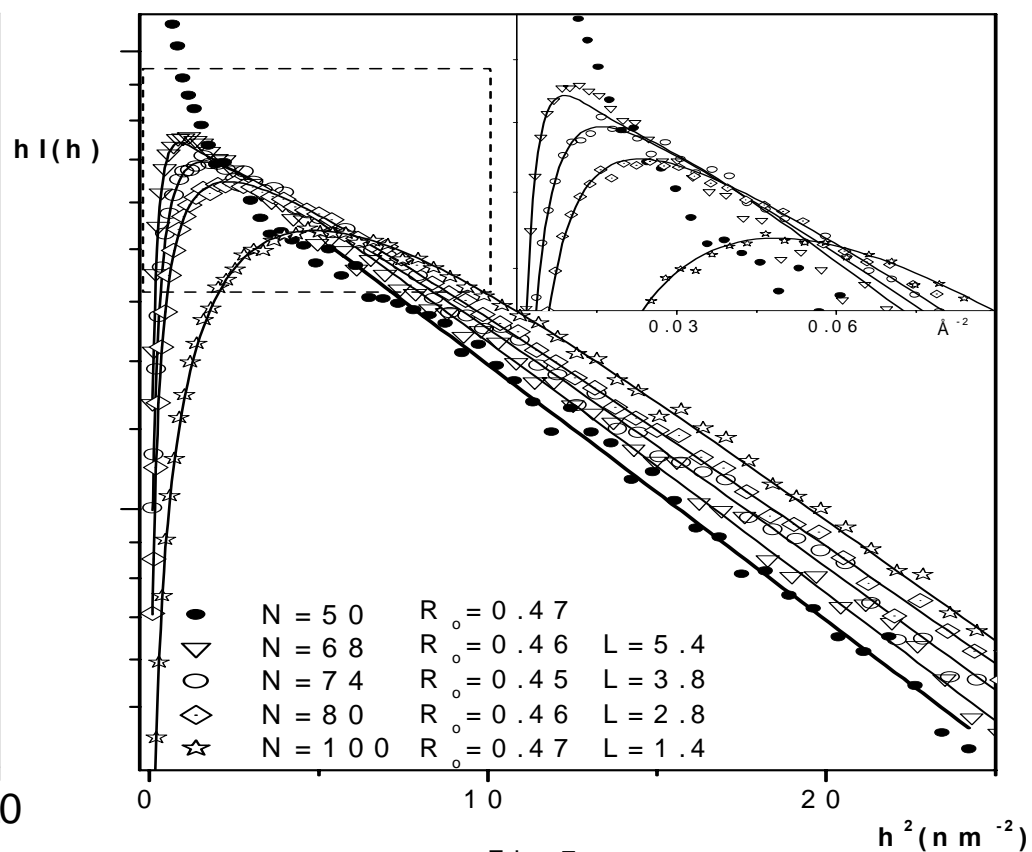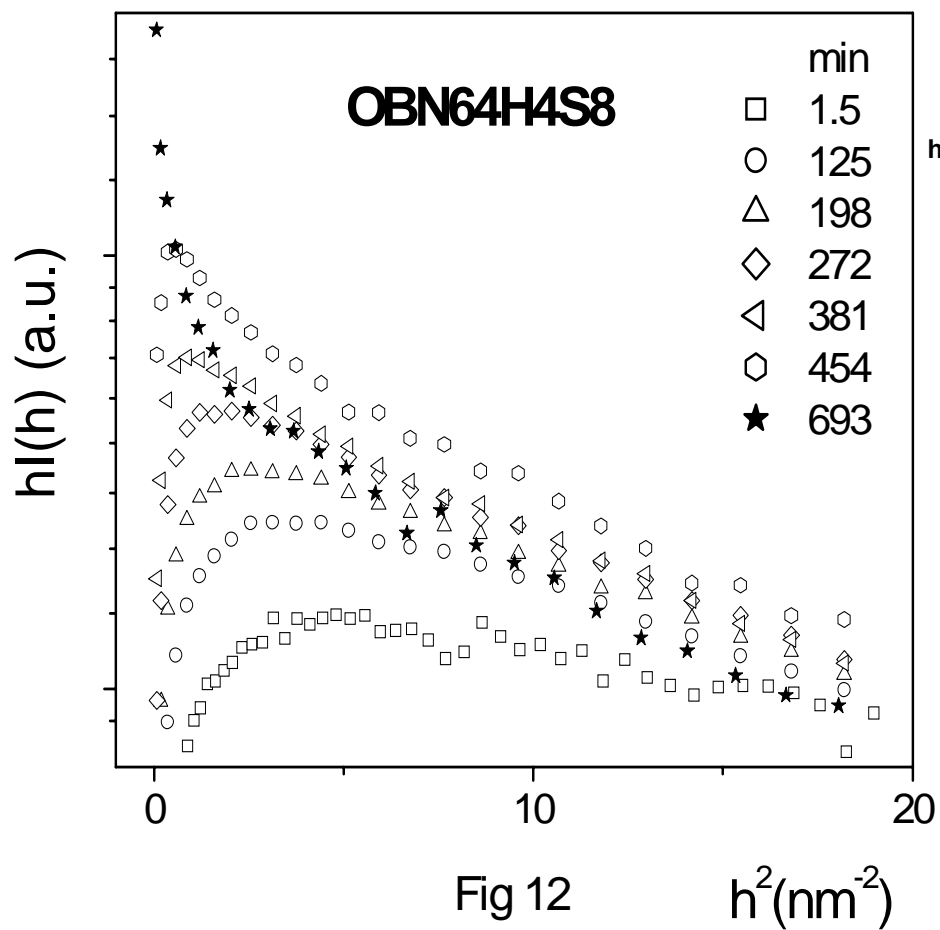
Alternative procedure for the determination of the fractal dimension from SAXS results

$$I(0) \propto M \qquad M \propto R_g^D \qquad I(0) \propto R_g^D$$

$$\boxed{\log I(0) = a + D.\log R_g}$$

R_g (determined from the slope)

Log I(q)

log.I(0)

q² (A⁻²)

$q^2 (A^{-2})$

Log I(0)

Slope =D

Log R_g
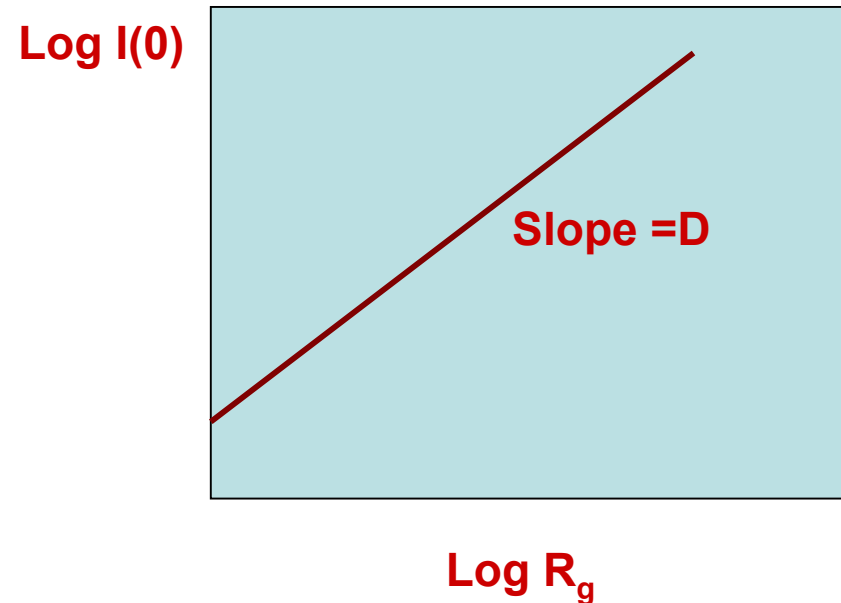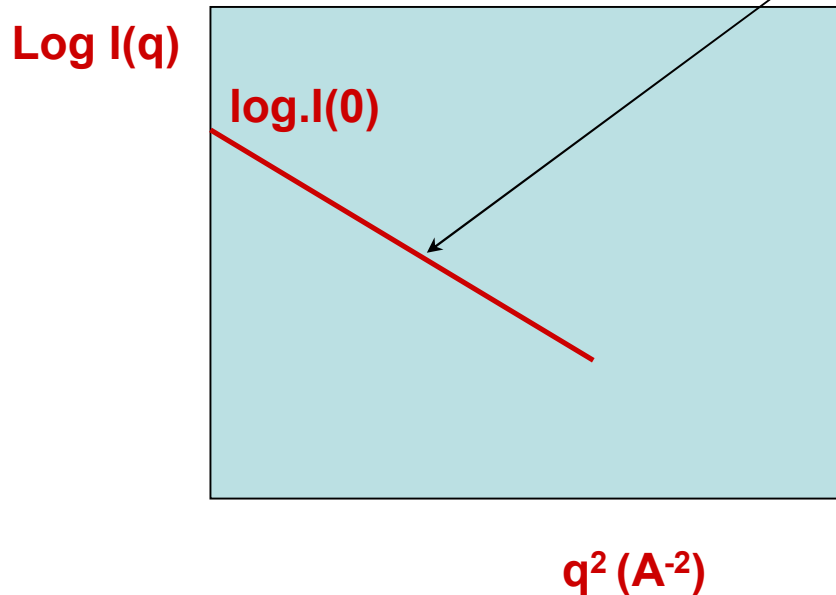
Mechanisms of aggregation of sulfato-zirconia colloidal solutions
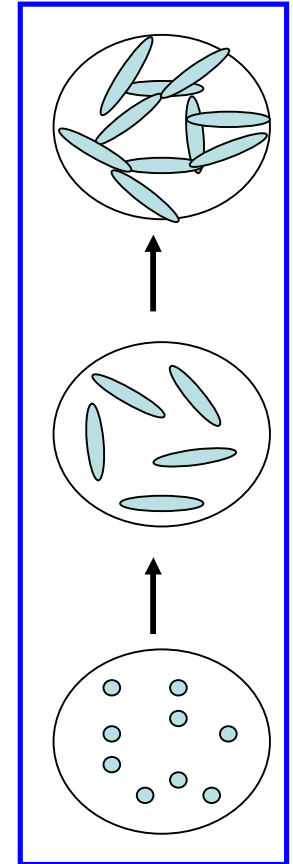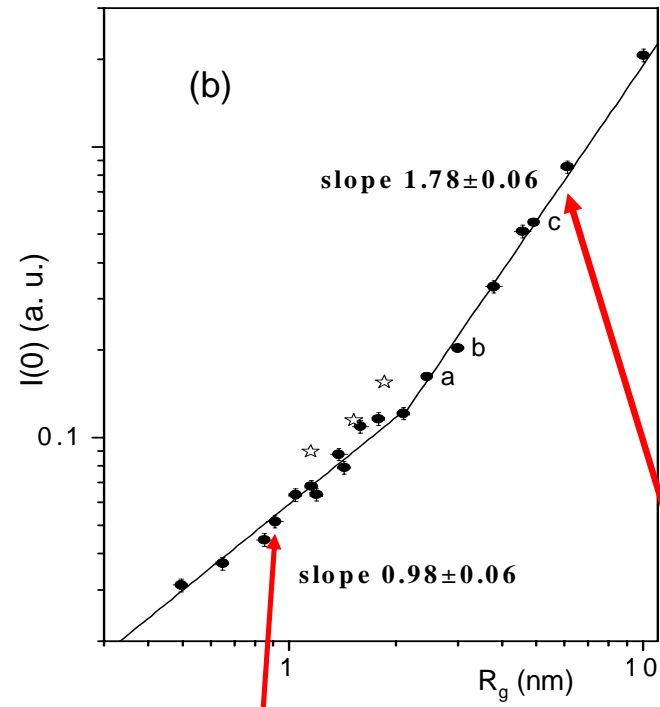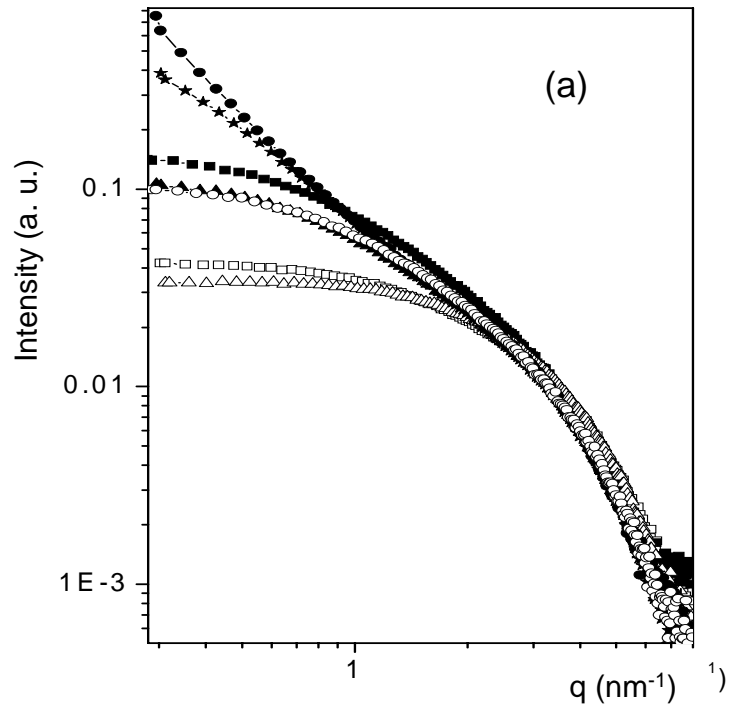
$$I(0) = b.Rg^D$$

$$\text{Log } I(0) = c + D.\log q$$

D=1:   Linear growth

D=1.78: Diffusion limited cluster agregation (DLCA)

Concentrated set of spherical nano-objects.
Short range order. Isotropic system
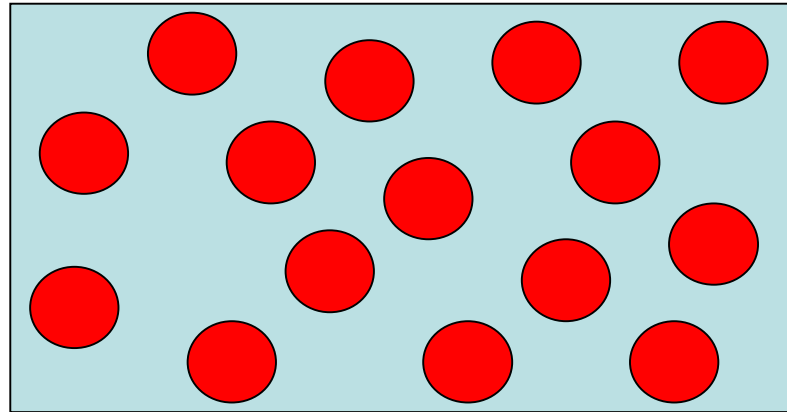
$$I(q) = N.I_1(q).S(q)$$

S(q) 1 for high q   (S(q)=1 for dilute systems)

Spherical nano-objects embedded in a solid matrix
Effects of high concentration

$$I(q) = N.I_1(q).S(q)$$
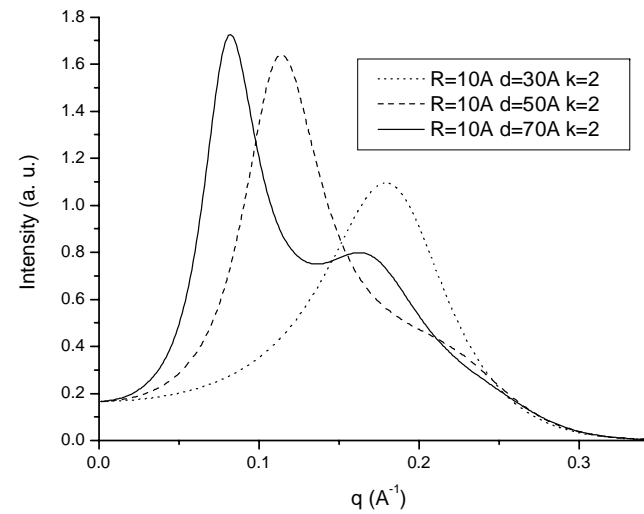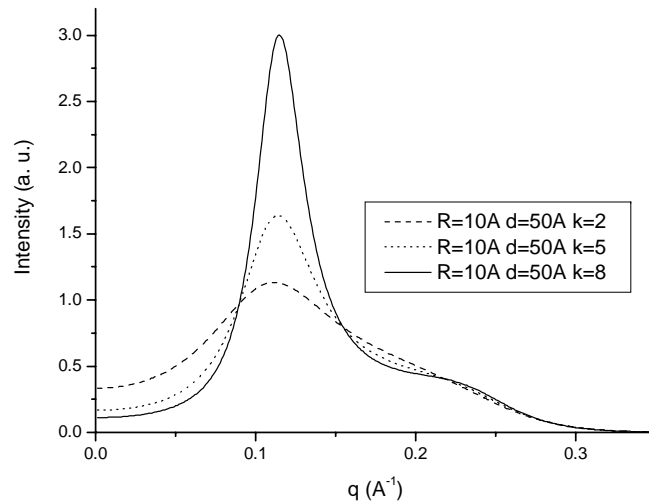
$$S(q) = \frac{1}{1 + k\Phi(qd)}$$

$$\Phi(qd) = 3\frac{\sin(qd) - qd\cos(qd)}{(qd)^3}$$

$$d = \frac{2\pi}{q_{max}}$$

Two-level structure
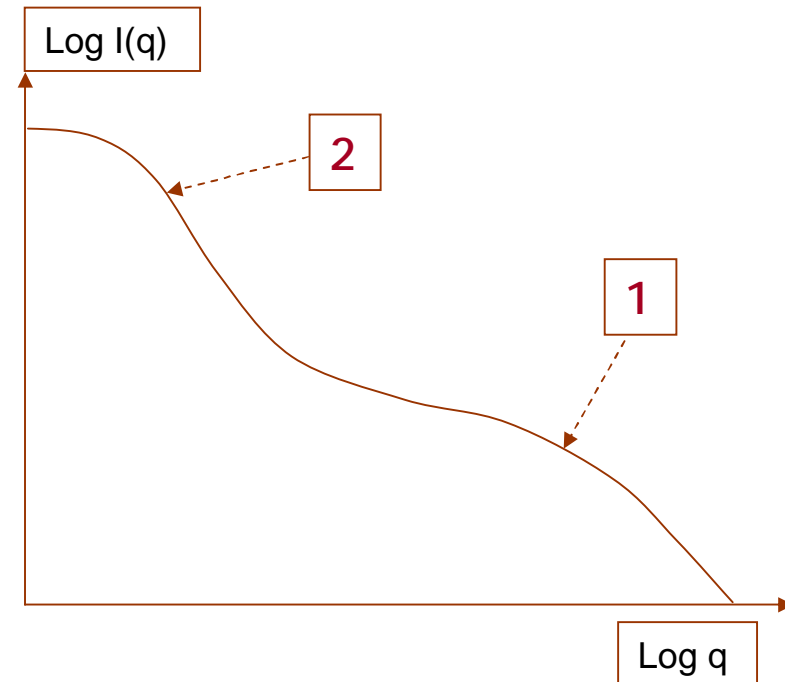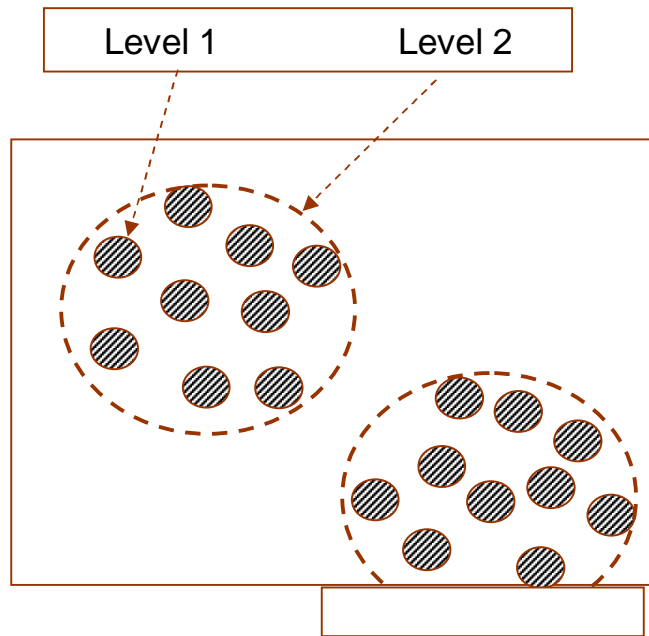
$$I(q) = \left[G_1 . e^{-\frac{1}{3}R_{g1}^2 q^2} + B_1 . e^{-\frac{1}{3}R_c^2 q^2} \left\{ \left[erf\left(qR_{g1} / 6^{1/2} \right) \right]^3 / q \right\}^4 \right] . + . \left[G_2 . e^{-\frac{1}{3}R_{g2}^2 q^2} + B_2 . \left\{ \left[erf\left(qR_{g2} / 6^{1/2} \right) \right]^3 / q \right\}^4 \right]$$

$$I(q) = \sum_{i=1}^{n} \left[G_i . e^{-\frac{1}{3}R_{gi}^2 q^2} + B_1 . e^{-\frac{1}{3}R_{g(i+1)}^2 q^2} \left\{ \left[erf\left(qR_{gi} / 6^{1/2} \right) \right]^3 / q \right\}^4 \right]$$

(Beaucage equation)

G. Beaucage et al Hybrids Organic-Inorganic Composites, ACSS. 97, 585 (1995).
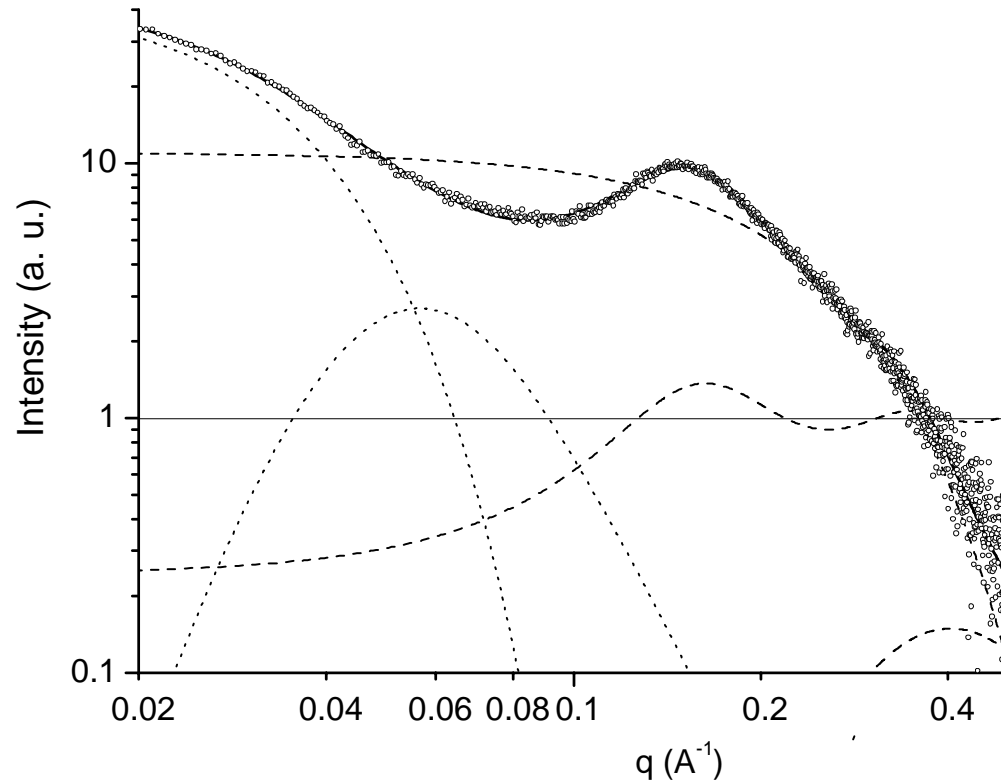
Fe(II) doped di-ureasil hybrids. Experimental scattering intensity from a sample containing 0.76 weight % Fe(II). The continuous line is the best fit of Beacauge equation to the experimental curve. The dashed lines indicate the Guinier and Porod contributions to the scattering intensity produced by siliceous clusters and the structure function (oscillatory curve). The point lines are the Guinier and Porod contributions to the scattering intensity yielded by the coarse domain.

N.J.O. Silva, K. Dahmouche, C.V. Santilli, V.S. Amaral, L.C. Carlos, V. Zea Bermudez, A.F. Craievich, J. Appl. Cryst. 36, 961-6 (2003).

Structure of self-organized nanoporous CTAB-based materials and their precursors

E. Terres (IMP, México), J. M. Dominguez (IMP, México)
and A. F. Craievich (IF-USP, Brasil). Under way (2004)

-The structure of nanoporous materials and their precursors was studied along the whole preparation procedure, starting from the initial sol containing H_2O + CTAB + NH_4OH + cosurfactant, until the final nanoporous solid obtained after TEOS addition, drying and calcination.

-The central issue of this investigation is the characterization of the effects of the composition on the structural features of the final nanoporous materials.

Sample without TEOS

Kinetics after TEOS addition (from 0 to 30 min)

q_1

$q_2 = 2.q_1$
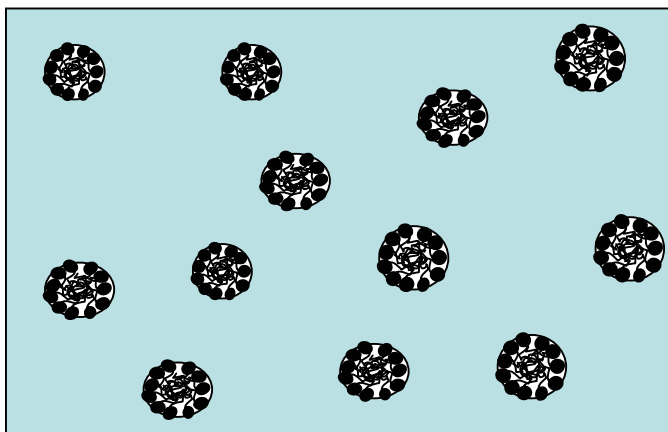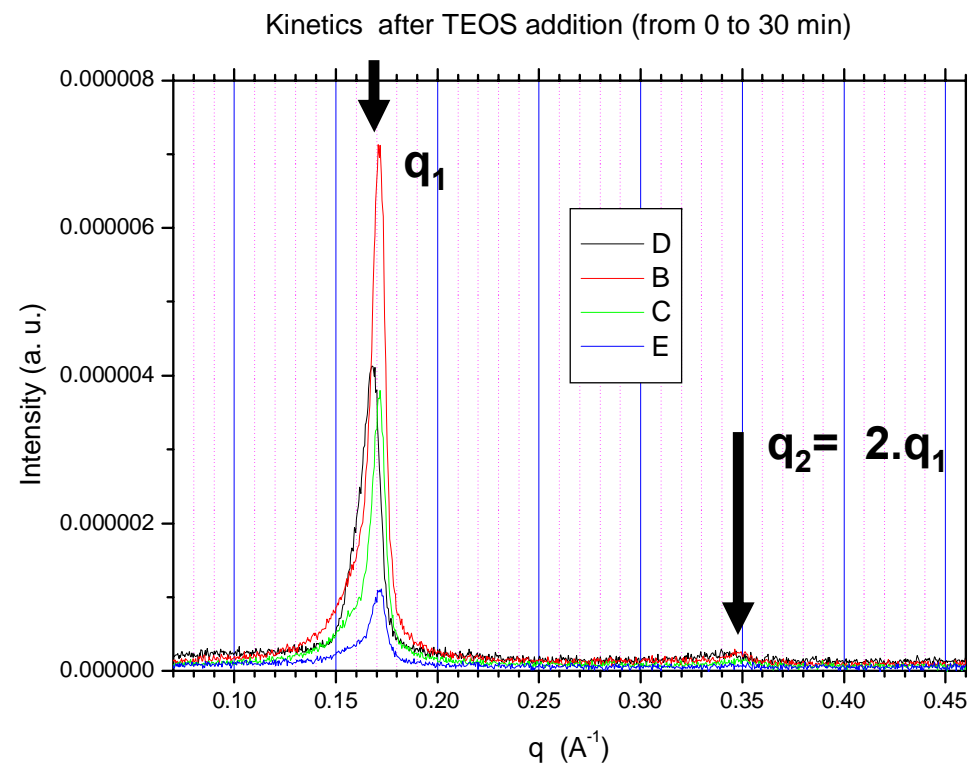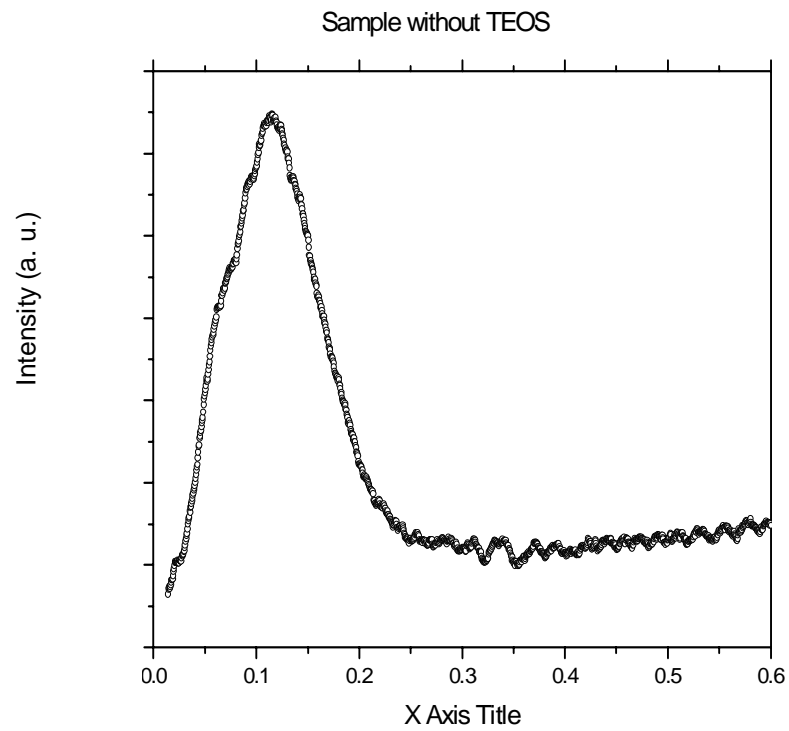
Effect of the amount of ethanol

Intensity (a. u.)

(4,8)
(4,6)
(4,4)
(4,2)

q (A^{-1})

q_1 ?? $3^{1/2}.q_1$ $2.q_1$

Ethanol conc.

Small-angle X-ray diffraction calcinados
H_2O + CTAB (4.5 w) + NH_4OH + X etanol + TEOS

Intensity (a. u.)

(4,8)
(4,6)
(4,4)
(4,2)

q (A^{-1})
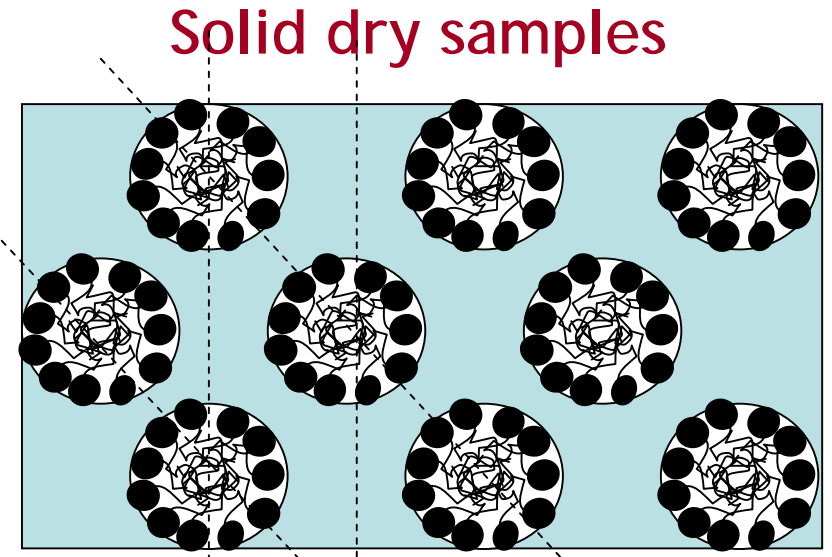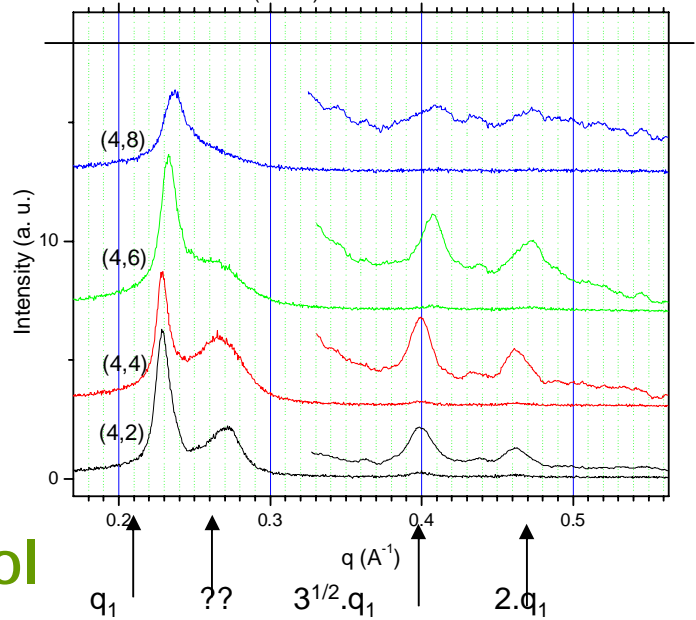
Solid dry samples

$d_1/3^{1/2}$

$d_1 = 27.5$ A
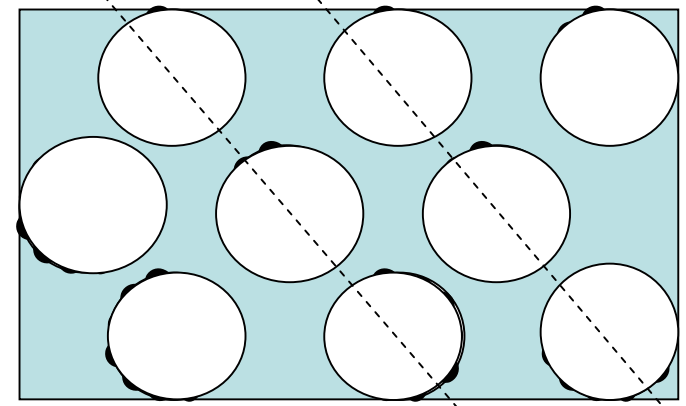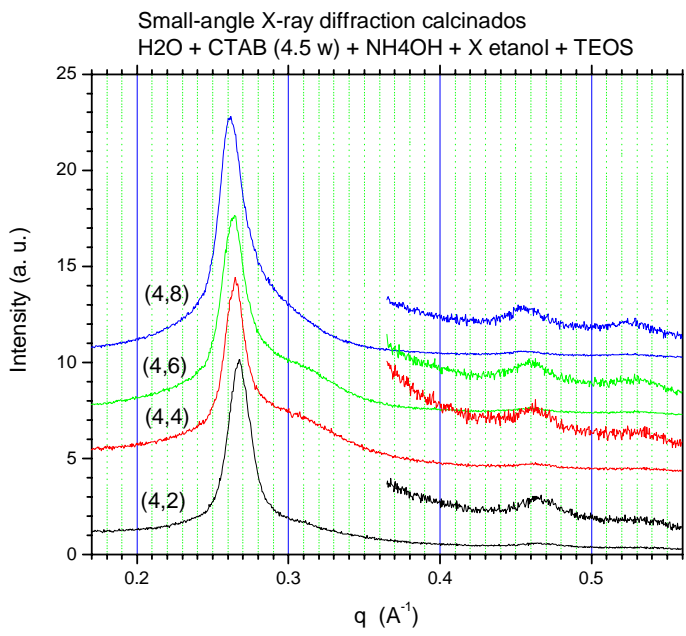
Calcined samples

23.5 A

Solid samples with different cosurfactants

Propanol
Methanol
Acetone

q (A^{-1})

Serie L Other cosurfactants

Acetone (4,2)
Acetone (4,6)
Methanol (4,2)
Methanol (4,6)
Isopropanol(4,2)
Isopropanol (4,6)

q (A^{-1})
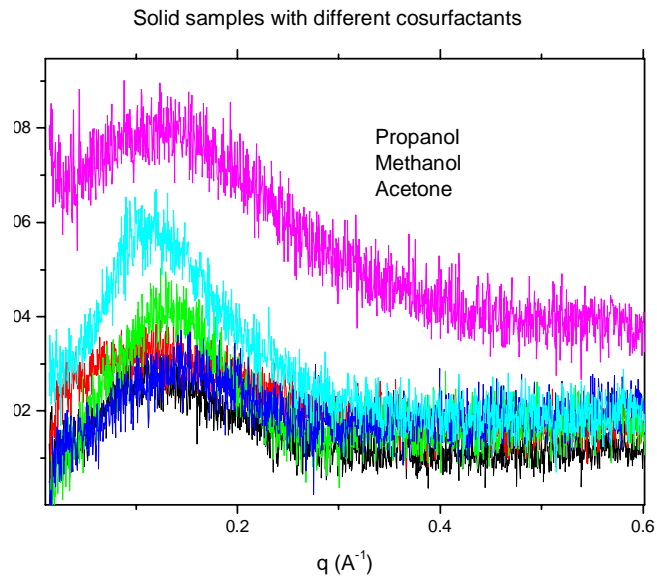
Effect of the nature of the co-surfactant

Methanol

Isopropanol

Acetone

Solid dry sample
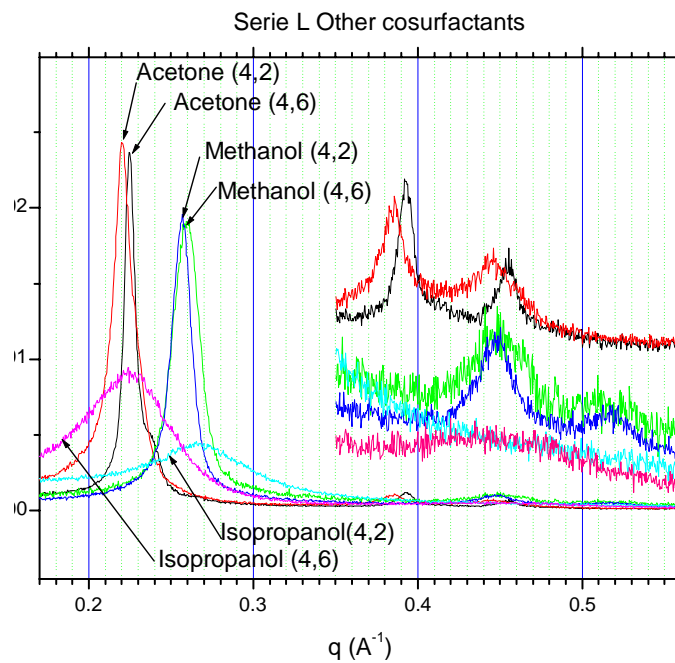
Solid calcined samples
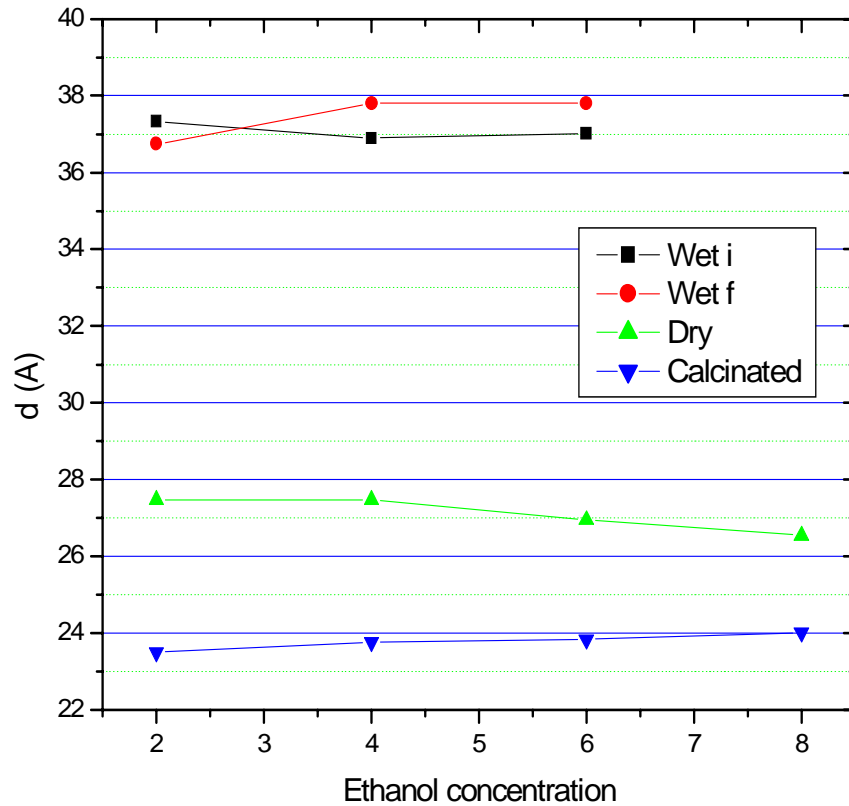
Effects of the nature of the co-surfactant and of the amount added on the plane spacing of the 2D lattice, in dry and calcined samples
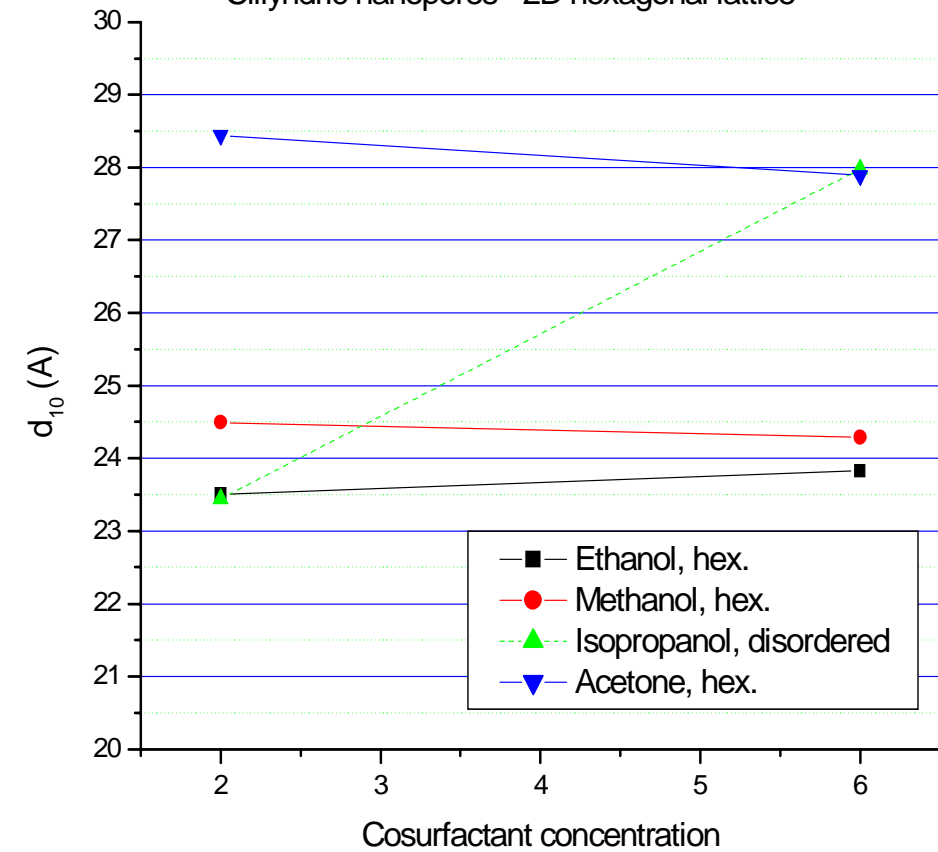
CONCLUSION

1) The sequence of structures during the transformation corresponding to the sample set A (H2O+CTAB(4.5 w%)+NH4OH+ethanol (x)+TEOS) is:
i) Before TEOS addition: disordered spherical micelles
ii) After drying: ordered (hexagonal) 2D arrangement of cylindrical micelles.
iv) After calcination: contracted ordered (hexagonal) 2D arrangement of cylindrical nanopores.

2) During calcination of the samples of set A, the geometric arrangement strongly contract but the geometrical features of the resulting system of cylindrical nanopores is approximately preserved. In addition to this phase, consisting of a ordered arrangement of micelles, another disordered phase coexists. The fraction of this disordered phase is reduced with the increase of ethanol content.

4) The final solid obtained from sols containing isopropanol is disordered (no 2D hexagonal arrangment of nanopores is observed).

5) The structural details of the final calcined solid strongly depend on the type of cosurfactant used and of their concentration.

Nanophase separation
and dynamical scaling
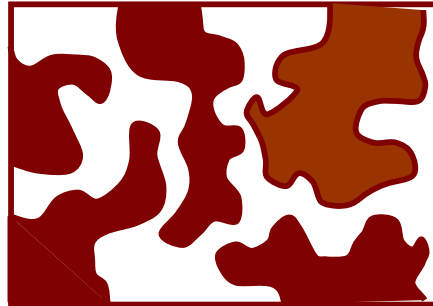
Nanophase separation
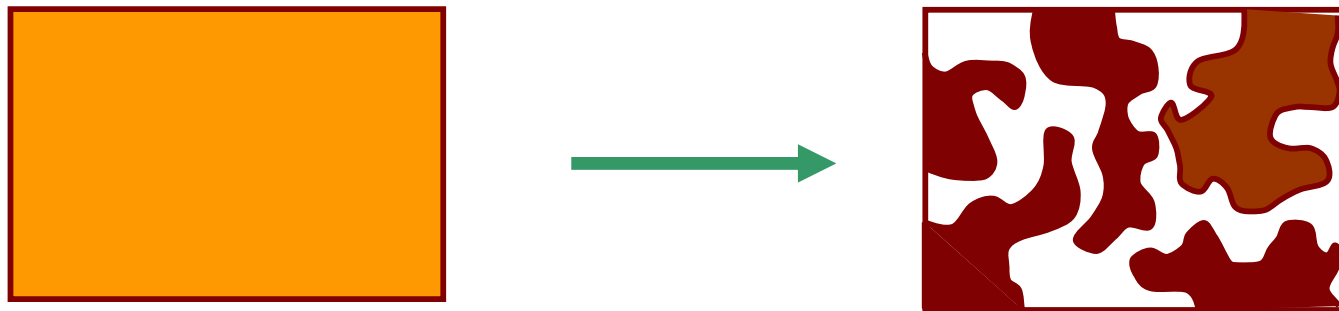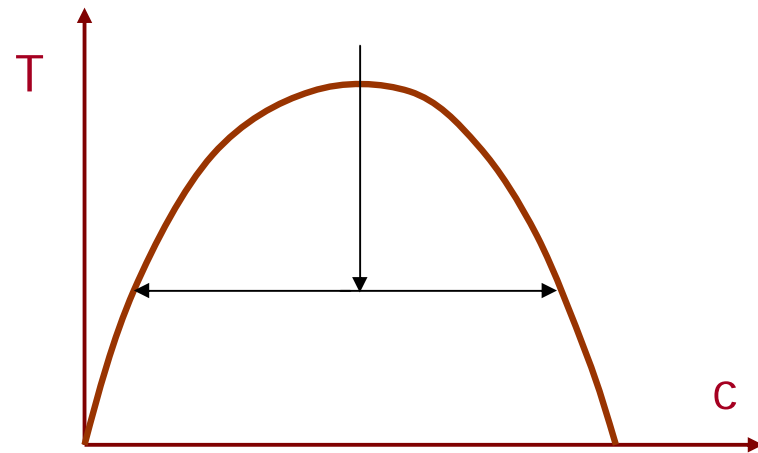
Dynamical scaling properties

Dynamical scaling property

$$F(x) = I(q) \cdot q_1^3$$

I(q)

q

X = (q/q_1)
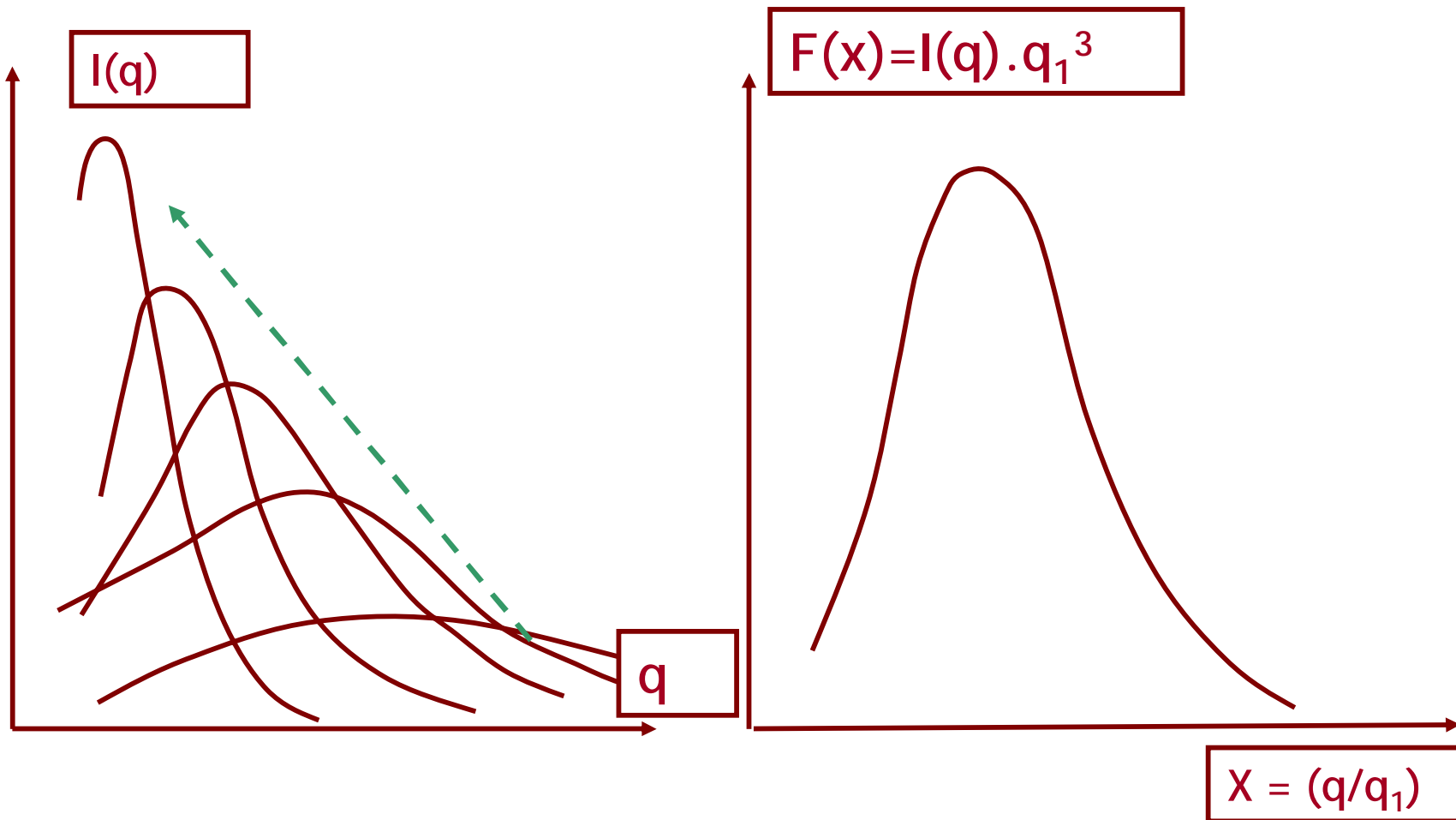
J.L. Lebowitz, J. Marro, M. K. Kalos, Acta Met. 30, 297-310 (1982).

F(x) is time independent !
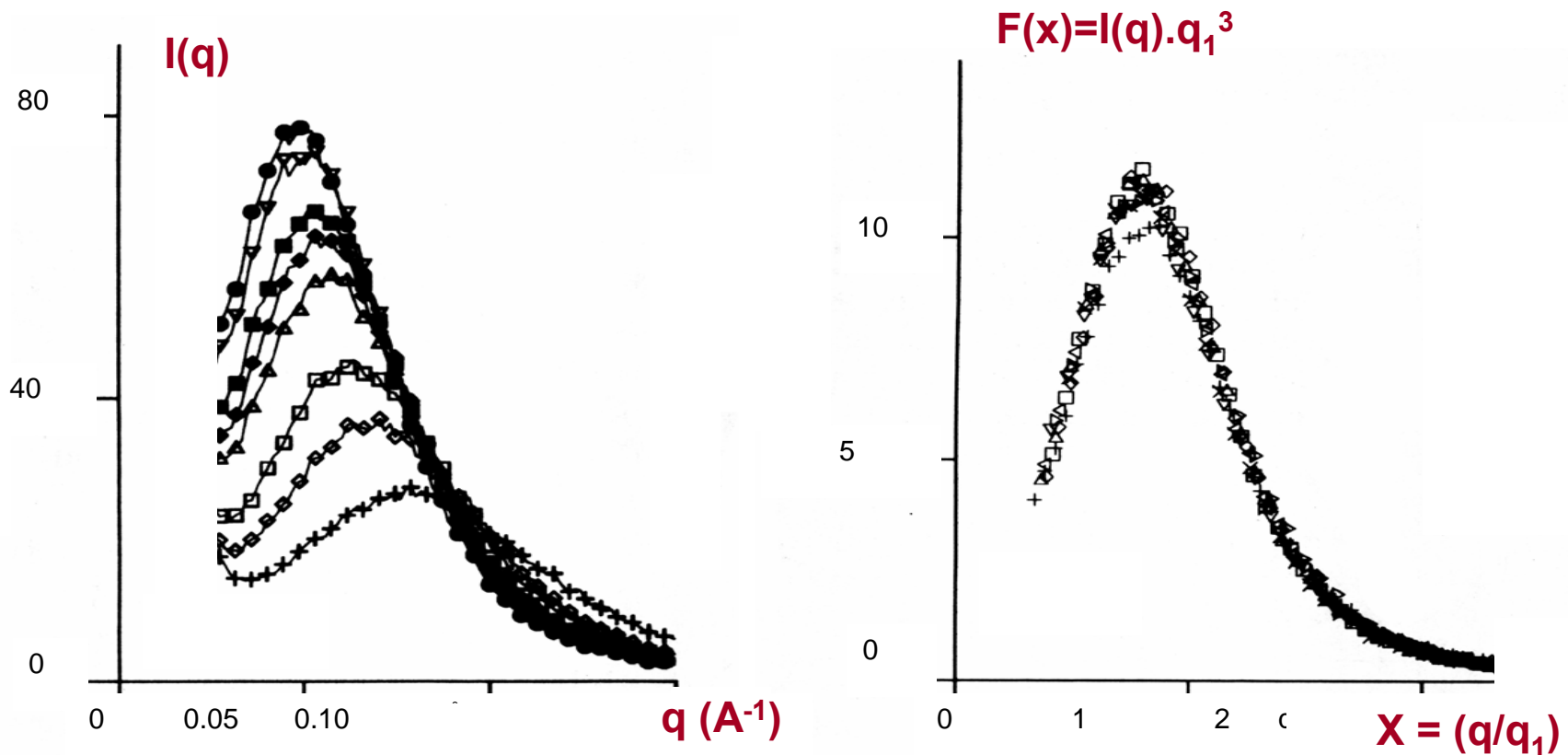
SnO2 based porous xerogels. (left) Scattering intensity curves corresponding to a nanoporous SnO_2 xerogel held at 400C during increasing periods of time from 4.5 min. (bottom) up to 62.5 min (top). (right) Same curves plotted as $[S(q,t)q_1^3]$ versus (q/q_1).

C.V. Santilli, S.H. Pulcinelli, A.F. Craievich, Phys. Rev. B 51, 8801-9 (1995).
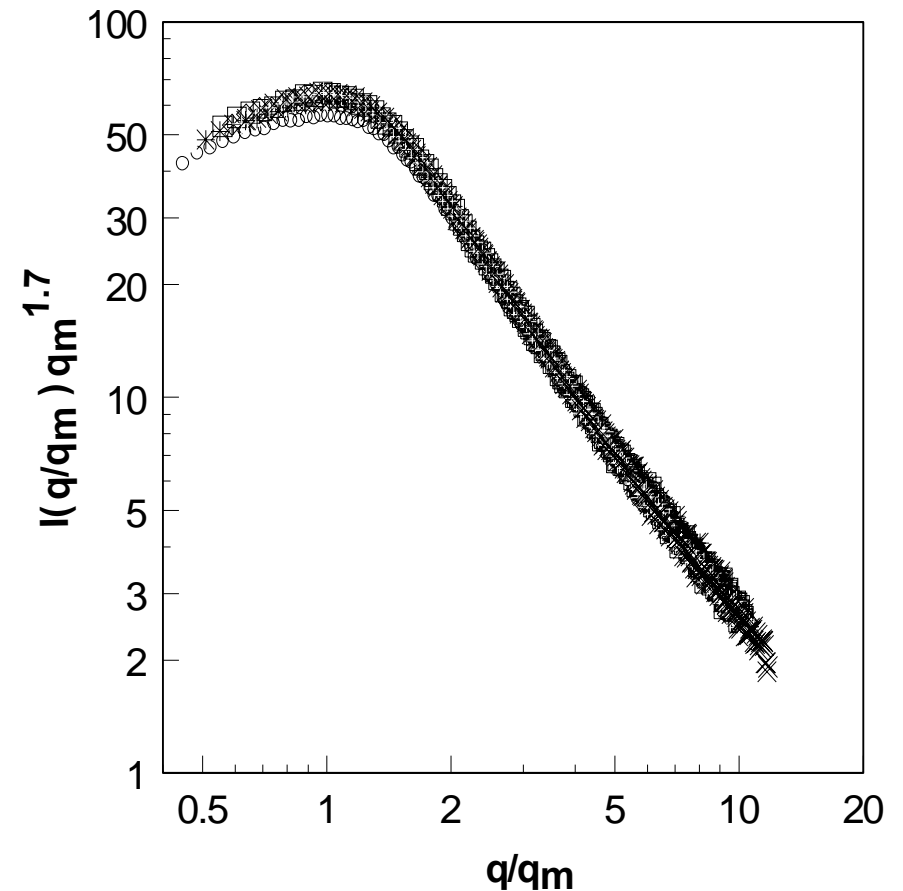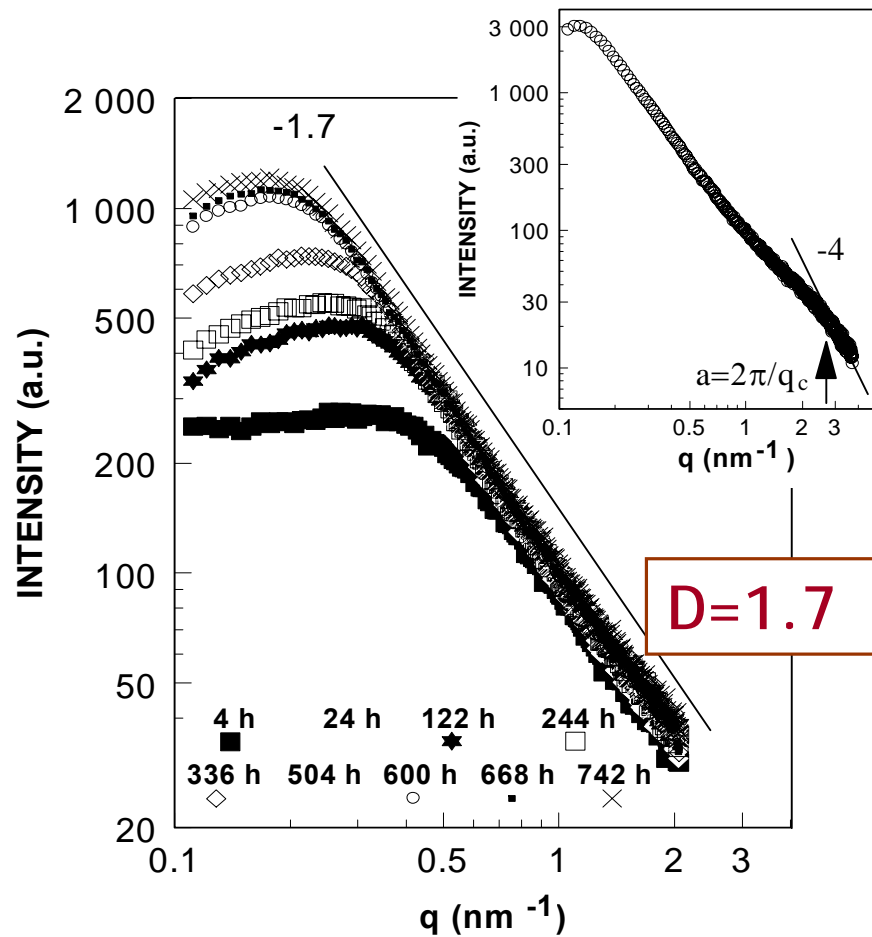
Scattering intensity curves (left) are re-plotted at right as
$[I(q)q_m^{1.7}]$ versus (q/q_m), q_m being the q value corresponding
to the maximum of the scattering curves

A. Lecomte, A. Dauger, P.J. Lenormand, J. Appl. Cryst. 33, 496-9(2000).

Remarks

The dynamical scaling property has been experimentally verified for the advanced stages of transformation processes occurring in many systems, such as crystalline-crystalline, glass-glass and porous nanomaterials.

The scaling property was also verified to be valid for the process of fractal growth in a zirconia based sol; in this case it was used in the definition of the the scaled function $F(x)=I(q).q^z$, the exponent $z=D$ (D: fractal dimension) instead of $z=3$.

The use of the situ synchrotron SAXS technique was demonstrated to be useful in order to precisely establish the actual time invariance of the scaled function $F(x)$ in a number of materials.

"When scientists have learned how to control the arrangment of matter at a very small scale, they will see materials take an enormously richer variety of properties"

Richard Feynman (1959)
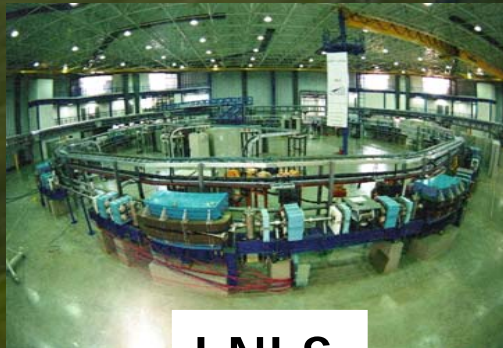
LNLS

Nanomaterials
- Size
- Shape
- Processes
  - S.R.

and
- Properties

A new material ?

Synchrotron SAXS Study of the Mechanisms of Aggregation of Sulfate Zirconia Sols

P. Riello,[*,†] **A. Minesso,**[†] **A. Craievich,**[‡] **and A. Benedetti**[†]

Dipartimento di Chimica Fisica, Università di Venezia, Venezia, Italy, and Instituto de Física, Universidade de São Paulo, São Paulo, Brazil

Received: November 11, 2002

This is a systematic investigation, using in situ synchrotron small-angle X-ray scattering, of the mechanisms of aggregation of sulfate zirconia sols under different preparation conditions. We have studied the effects of the variations of acid, water, and sulfate contents on the process of aggregate growth. These effects were investigated using open and sealed sample cells. It was observed that two clearly different mechanisms govern the aggregation at the beginning and at advanced stages of the process. In the early stages, small needle-shaped clusters are formed. They have a time independent cross-section and progressively grow by increasing their length. At advanced stages, the initially isolated needle-shaped clusters start to build up a 3D structure, their aggregation being governed by the classical mechanism of diffusion-limited cluster aggregation (DLCA). The experimental results also suggested an effect of sulfate concentration on the structure of the aggregates. Even though the structures of the final sols vary markedly due to differences in the chemical and physical preparation conditions, our experimental results suggest that a single and remarkably simple model explains the aggregation process for all the studied solutions.

1. Introduction

The physical and chemical properties as well as the structure of the final products obtained by the sol−gel procedure strongly depend on the preparation conditions. Two of the most important parameters in the sol−gel process are the amount and type of catalyst used and the hydrolysis ratio. The hydrolysis ratio is defined as the number of water moles per mole of precursor. The choice of the catalyst is particularly important in controlling the hydrolysis of zirconium alcoxide because the high reactivity of the precursor in the presence of even a small amount of water leads to a fast precipitation of zirconium hydroxide instead of forming a homogeneous gel.

The simplest way of controlling aggregation and gelation processes in a zirconium alcoxide alcohol solution is the addition of a small amount of an inorganic acid (HNO_3, HCl) to the solution. The acid modifies the relative rates of hydrolysis and condensation, thus determining the type of product formed.[1] Moreover, previous authors,[2] investigating the gelation of acid-catalyzed TEOS solution with $[H_2O]/[TEOS] = 2$ in order to compare the nature of sols prepared in open and sealed cells, have also established that spinnability occurs in the former but is negligible in the latter, although both sols were prepared with the same starting composition. This indicates that, even if the nature of polymers or clusters formed in the initial stages of reaction is identical, the structural evolution in the sols may become quite different when the amount of solvent evaporated from the solution is varied. Finally, it is also well-known that the type of solvent can control the alcoxide reactivity.[3]

Because of their potential as a promising contribution to the achievement of a new generation of catalysts for environmentally friendly processes, sulfated zirconia-based materials have recently been studied by many authors.[4−9] Sulfated zirconium oxides prepared by the sol−gel procedure lead, after the thermal activation treatment, to different final products (with different crystal structures and specific surface areas) depending on water and catalyst contents.[10] In previous studies of similar systems, it was established that the aggregation of monomers in the sol phase leads to cylindrical aggregates that eventually grow and build up complex fractal objects.[11−16]

The aim of this work is to systematically investigate, using the small-angle X-ray scattering (SAXS) technique, the effects of the variation of several chemical parameters, such as $[HNO_3]/[Zr(OPr)_4]$ and $[H_2O]/[Zr(OPr)_4]$ molar ratios and $[H_2SO_4]/[Zr(OPr)_4]$ weight ratio concentration, on the mechanisms of aggregation of sulfate zirconia prepared by the sol−gel method. The experimental study was performed by in situ SAXS, using sealed and open sample cells, to verify whether the formation of final products with completely different nanostructural properties can be explained in terms of a unified mechanism of growth.

2. SAXS Analysis

2.1. Relevant Equations. To analyze the experimental SAXS curves corresponding to a diluted set of colloidal particles that develop during the first stages of aggregation, we have applied the Zimm equation

$$I(h) = I(0)/(1 + h^2R_g{}^2/3) \qquad (1)$$

where R_g is an average radius of gyration[17] of the cluster or aggregate and $h = (4\pi/\lambda)\sin\theta$ is the modulus of the scattering vector, λ being the X-ray wavelength and θ half of the scattering angle. The Zimm equation applies to the low h range of the SAXS intensity produced by randomly oriented colloidal objects. We preferred eq 1 to the Guinier equation $[I(h) = I(0)\exp(-h^2R_g{}^2/3)]$ because the Zimm equation fits our experimental SAXS intensity curves within a wider h range.

We have determined an average radius of gyration, R_g, of the colloidal clusters from the slope of the linear part of the Zimm plot $[1/I(h)$ versus $h^2]$ and the value $I(0)$ by linear extrapolation to $h = 0$.

* Corresponding author. E-mail: Riellop@Unive.it
† Università di Venezia.
‡ Universidade de São Paulo.

Mechanisms of Sulfate Zirconia Sol Aggregation

J. Phys. Chem. B, Vol. 107, No. 15, 2003 **3391**

In the case of acicular or rod-like particles with a length L that is much larger than their diameter, a modified Guinier equation can be applied:

$$hI(h) \propto \exp(-h^2 R_c^2/2) \tag{2}$$

with R_c being an average radius of gyration of the cross-section. Equation 2 applies within the h range defined by $2\pi/L < h < 1/R_c$.[18] The lowest h value in this range, when applied to experimental SAXS curves, yields an estimate of the cylinder length L. If the elongated particles are assumed to have a cylindrical shape, the geometrical radius of the cross-section is $R_0 = \sqrt{2}\, R_c$.[18]

The SAXS intensity of a dilute set of cylindrical particles, with radius R_o and variable length L with distribution $P(L)$, is given by (Appendix eq A10)

$$I(h) = \frac{I(0)}{\langle L^2 \rangle} \int_0^{\pi/2} \int_0^{\infty} P(L) L^2 \times$$
$$\frac{\sin^2(hL\cos\vartheta/2)}{(hL\cos\vartheta/2)^2}\frac{4J_1^2(hR\sin\vartheta)}{(hR\sin\vartheta)^2}\sin\vartheta\,\mathrm{d}\vartheta\,\mathrm{d}L \tag{3}$$

We have assumed that the distribution of cylinder lengths, $P(L)$, can be described, as in a number of previous polymer investigations,[19−21] by the Schultz function which is expected to be the "most probable" in aggregation of linear polymers:

$$P(L) = \frac{1}{\Gamma(z+1)}\left(\frac{z+1}{\langle L \rangle}\right)^{z+1} L^z\, e^{[-(z+1)L/\langle L \rangle]} \tag{4}$$

with $z > -1$.

2.2. Scattering Intensity by Aggregates. To characterize the aggregation of colloidal particles, it is insightful to examine the dependence of the mass of the aggregates, M, on their radius of gyration, R_g. In many published theoretical and experimental investigations the simple equation

$$M \propto R_g^D \tag{5}$$

holds. R_g, determined by SAXS measurements, is actually an electron density radius of gyration but it also corresponds, as a good approximation, to the mass density radius. The exponent D provides information on the geometry of the aggregates and on their mechanism of growth (e.g., rods: $D = 1$, platelets: $D = 2$, mass fractals: $1 < D < 3$).

The SAXS measurements allow one a direct evaluation of the parameters M, R_g, and D. Since the SAXS intensity extrapolated to $h = 0$, $I(0)$, is proportional to the mass of the aggregates, M, (Appendix),[22] eq 5 may also be written as

$$I(0) \propto R_g^D \tag{5a}$$

The extrapolated intensity, $I(0)$, and the average radius of gyration of the aggregates, R_g, are often determined by using the Guinier equation or, as in this paper, by applying the Zimm equation (eq 1). The validity of eq 5 when applied to a set of nonidentical aggregates is discussed in the Appendix.

Under suitable conditions, many types of colloidal aggregates exhibit a fractal structure. For these objects, named mass fractals,[23,24] the exponent D may have noninteger values within the interval $1 < D < 3$.[23−25] The values of the fractal dimension D obtained experimentally by SAXS may be compared to those obtained by computer simulation based on different growth models (e.g., diffusion-limited aggregation, DLA, reaction

limited aggregation, RLA).[26−33] Therefore, SAXS is the proper technique for characterizing the mechanisms of growth in solutions of colloidal particles.

From the mathematical point of view, fractal structures are self-similar and their relevant features are independent of the scale of observation, i.e., the self-similarity is conserved through an infinite scale range. However, in real systems, the range of self-similarity is limited by the nonzero size, a_0, of the smallest "building block" (i.e., monomers) and by the finite overall size, R_g, of the fractal aggregate. Consequently, self-similarity can only be observed in nature within a limited range of sizes. To our knowledge, three orders of magnitude of self-similarity is the widest range experimentally observed up to now.[34]

For mass fractal aggregates, the SAXS intensity within the range $1/R_g < h < 1/a_o$ is given by[35]

$$I(h) \propto h^{-D} \tag{6}$$

Consequently, over the mentioned h range, the $\mathrm{Log}[I(h)]$ vs $\mathrm{Log}[h]$ plot exhibits a linear behavior with slope $-D$. This approach is the most frequently used procedure to obtain the exponent D from SAXS measurements. Avnir et al.[36] have recently underlined that, in many experimental studies, the empirical fractal dimension D obtained in such a way was determined on a scale range that spans only 0.5 to 2.0 decades. His review of data analysis, covering about 100 articles reported in the literature, exhibits a histogram centered at about 1.3 decades. This scale range is often not wide enough to clearly establish the fractal nature of the investigated structures.[36]

Even if the aggregates grow by a well-defined mechanism, they may stop their growth and remain rather small so that the mechanism of aggregation cannot be recognized from their structural features. In these cases, the use of eq 5a allows one to study the aggregation from the very beginning of the growth process, well before the formation of large fractal aggregates. The characteristic exponent D, obtained by using eq 5a during the growth process, was demonstrated to be equal to the exponent obtained by using eq 6 for the fractal structure that is formed at the final stages of growth.[37] We would like to emphasize the usefulness of eq 5a in order to directly and easily compare different samples prepared under different conditions and exhibiting either fractal or nonfractal structures. This analysis also allows one to directly verify whether the growth of the aggregates in a sol with a common parent propoxide is governed by the same mechanism along the whole aggregation process.

3. Experimental Section

3.1. Samples. In the sol−gel synthesis of all the samples studied here, sulfuric acid was immediately added to zirconium-n-propoxide, used as precursor, to include sulfate groups in the oxide gel network. Two different procedures consisting of one-step (A) and two-step (B) hydrolysis were used.

In the one-step hydrolysis procedure[38,39] the zirconium propoxide/H_2SO_4/(k)-propanol solution was hydrolyzed with a H_2O/HNO_3/(k)-propanol solution ($k = 1,2$). The amounts of HNO_3 and H_2O were chosen in order to vary the molar ratios $N = [HNO_3]/[Zr(O\,n\text{-Pr})_4]$ from 0.5 to 1, and $H = [H_2O]/[Zr(O\,n\text{-Pr})_4]$ from about 1 up to 4 (see Table 1a). A few compositions with different H_2SO_4 contents were also prepared. The complete set of compositions investigated using sealed cell is reported in Table 1 (a and b). All samples were prepared using 2-propanol, except the composition reported in the second line of Table 1a ($H = 2$) and the sample CN100H130S32 that were prepared also using 1-propanol. Two

TABLE 1: Compositions Investigated Using Sealed Cell[a]

A. Samples with Same H_2SO_4 Content

H	N				
	0.5	0.68	0.74	0.8	1.0
1		CN68H100S8			CN100H130S32[b]
2	CN50H200S8	CN68H200S8	CN74H200S8	CN80H200S8	CN100H200S8
3		CN68H300S8			CN100H300S8
4	CN50H400S8	CN68H400S8	CN74H400S8	CN80H400S8	CN100H400S8

B. Samples with Different H_2SO_4 Content

S	N	
	0.68	0.8
0	CN68H200S0	CN80H200S0
2	CN68H200S2	
8	CN68H200S8	CN80H200S8
32	CN68H200S32	

[a] The first letter C of the labels indicates the cell type (Closed). N, H, and S codes indicate $[HNO_3]/[Zr(OPr)_4]$ mol %, $[H_2O]/[Zr(OPr)_4]$ mol %, and the H_2SO_4 wt %, respectively. All the sols were prepared using method A (see main text). [b] The sulfuric acid content of this solution is 32 wt % and the water content ($H = 130$) is due to the water contained in the acids.

sols with composition N80H400S8 and N68H400S8 were also studied in an open cell (first code O) and prepared with the methods A and B, respectively (samples ON80H400S8 and OBN68H400S8). To follow the time evolution during both hydrolysis stages, three additional samples were studied (OBN64H400S8, OBN90H400S0, and OBN100H400S0).

In the two-step hydrolysis procedure,[40−42] only the desired amount of HNO_3 was initially added to the sulfated precursor solution of zirconium propoxide/H_2SO_4/(k)-propanol. In the early stage, the reaction took place with a sub-stoichiometric amount of H_2O (the water contained in the HNO_3 and H_2SO_4). Finally, the remaining water was added up to the desired $H = [H_2O]/[Zr(O\,n\text{-}Pr)_4]$ molar ratio of 4. All of the starting solutions are 0.45 M in alcohol.

3.2. SAXS Procedure. As soon as the hydrolyzing solution was added to the sulfated precursor, the sol was introduced into a thermostatic cell installed in a SAXS setup for in situ measurements during aggregation. About two minutes elapsed between the addition of the hydrolyzing solution and the beginning of SAXS measurements. Measurements were carried out using both open and sealed cells.

The SAXS experiments were conducted at the National Synchrotron Light Laboratory (LNLS), Campinas, Brazil, using a monochromatic X-ray beam ($\lambda = 1.609$ Å) that also focuses the beam horizontally and a position-sensitive X-ray detector for scattering intensity recording. The modulus of the scattering vector h covered the range from 0. 2 up to 5.5 nm^{-1} for the open sols and from 0.3 up to 9.5 nm^{-1} for the sealed ones. The open sols were studied using a cell with Mylar windows, sealed sols using a cell with mica windows.[43]

The parasitic scattering intensity (mainly produced by the cell windows) was subtracted from the total experimental intensity. The SAXS curves were normalized with respect to (i) the decreasing intensity of the incoming synchrotron beam and (ii) the variable X-ray absorption of the sol in open cell. We have performed the correction of all the scattering intensity curves in order to compensate for small differences in sensitivity over the whole window of the position-sensitive detector. The scattering intensities did not need any desmearing process because the geometry of the beam was nearly point-like and the width of the detector window used was very small. Eventual effects at low h values are small and within the statistical error bars. All SAXS intensities from sols in sealed cell are in the same relative scale because the thickness of the cell remained constant for all samples and along the whole aggregation

process. This last consideration does not apply to the sols in the open cell because their thickness slightly changed from one sample to another. Consequently, the relative intensities of different sols are not in the same scale. The SAXS intensity produced by each solvent (1 or 2-propanol and acids) was measured and taken into account in the data fitting procedure or subtracted from the total scattering intensity before analysis.

The sols studied in the sealed cell were prepared using method A (one-step procedure). The advantage of using a sealed cell is that it enables the control of the chemical composition of the solution. In the open cell, the concentration of the sol increases with time due to the evaporation of the solvent and there is a slow, but continuous, absorption of water from the atmosphere.

The kinetics of aggregation for sealed systems is very fast, especially in the early stages, except in the sols with a very high H_2SO_4 content (32 wt %). This prevented us from characterizing the aggregates from the beginning of the growth process. In this case, only sols that had reached their final state were studied by SAXS. On the other hand, the aggregation process of sols prepared by method B (two-step procedure) in an open cell, is relatively slow, so time-resolved SAXS measurements were possible. These series of measurements allowed us to characterize the structure of the aggregates from the very beginning of the aggregation process until the sol−gel transition.

4. Results and Discussion

SAXS measurements were carried out using a sealed or an open cell during the aggregation process of a number of sols with different compositions. Sealed sols reach an equilibrium state that is related to the initial preparation parameters. The open systems reach, in all cases, final states different from those of sealed systems, even if the initial solutions have the same nominal composition. This difference comes from the variation of the composition due to the absorption of water from the atmosphere and the evaporation of the solvent as underlined in the previous paragraph. These findings illustrate the complexity of the phenomena involved in the process of production materials by the sol−gel procedure. As a matter of fact, a little variation of one of the preparation parameters may produce final products with very different features. As a consequence it has been difficult, up to now, to establish a unified description for the mechanisms that control these reactions. For this reason, it seemed worth looking for a common framework able to describe different mechanisms of growth, yielding either fractal or non-
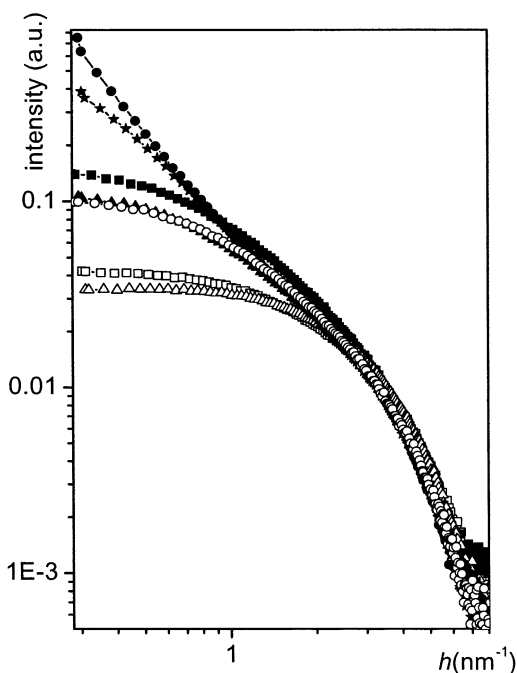
Mechanisms of Sulfate Zirconia Sol Aggregation

J. Phys. Chem. B, Vol. 107, No. 15, 2003 **3393**

Figure 1. Scattering intensities corresponding to a few selected sealed samples listed in Table 1a. □ CN68H100S8; ■ CN100H130S32; △ CN100H200S8; ▲ CN68H200S; ○ CN100H400S8; ● CN68H400S8; ★ CN100H300S8.

Figure 2. Plot of $I(0)$ vs R_g corresponding to the final states of all sealed samples, listed in Table 1a and 1b, with different H_2SO_4 contents. The circles correspond to $S = 0$, 2, and 8 and the stars to $S = 32$. Samples a, b, and c are particular samples described in the main text.

fractal structures, for different preparation conditions. To do that, we have separated the structural aspects of the aggregates from the kinetic process[11,12] that is related to the growth of the polymeric network.

4.1. Sols in Sealed Cell. Since the aggregation process of the studied sols in sealed cells is quite fast, we have only characterized their final quasi-equilibrium state for the different compositions listed in Table 1. This final state does not exhibit any further significant structural transformation within the time scale of our experiments. The scattering intensity curves corresponding to a few studied sols are plotted in Figure 1.

The values of $I(0)$ and R_g corresponding to the different studied sols were determined using Zimm plots and plotted in Figure 2. We can see that the average radius of gyration of the final aggregates in the different sols ranges from 0.5 up to 10 nm. This wide range evidences the strong dependence of the final structure of the aggregates on the composition of the solution.

Since the comparison of different solutions with different chemical composition is very critical and may lead to systematic errors in the analysis, we will start with a preliminary discussion of several relevant issues. One of the difficulties to be faced concerns the comparison of the intensities $I(0)$ that, in addition to being proportional to the mass of the aggregates, are also proportional to the concentration of the monomers and to the contrast factor that depends on the electronic density of the solvent (Appendix). Thus it is important to evaluate these effects numerically and, if necessary, to introduce the appropriate correcting factors. To perform this analysis, we have divided all the investigated solutions in the two sets that are described below.

(i) Solutions with Same H_2SO_4 Content. The maximum variation in the electron density contrast factor, $\Delta\rho^2$, between the solvent and the clusters (constituted of zirconium hydroxide) for the set of sols with $S = 8$ wt % is less than 1.0%. The concentration variation for the same set is less than 2%. The combined effects of contrast and concentration lead to a variation
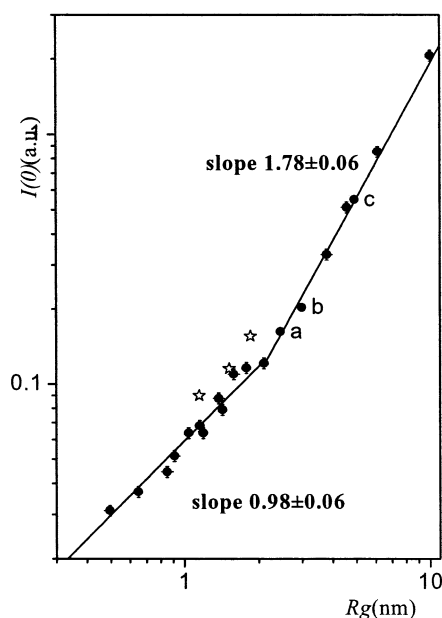
of $\pm1.5\%$ in SAXS intensity, which is always smaller than the estimated $\pm5\%$ statistical error in the evaluation of the intensity $I(0)$ by the extrapolation process. This error corresponds to the size of the symbols reported in Figure 2. The same arguments apply to the set of sols with $S = 32$ wt %.

Since the electron density of the solvent can be assumed to be nearly the same for all samples in this set, we have concluded that, in our case, the SAXS results corresponding to different sols with $S = 8$ wt % can be directly and quantitatively compared.

(ii) Solutions with Different H_2SO_4 Content. We have evaluated the eventual variation in electron density of the solvent assuming that sulfuric acid remains dissolved in it. The calculated difference between two samples with $S = 0$ wt % and $S = 32$ wt % is nearly 10%. Under this hypothesis the greater the acid content the higher is the electron density of the solvent, so that the contrast factor $\Delta\rho^2$ should be a decreasing function of H_2SO_4 content. Consequently, when comparing solutions containing clusters of the same size and increasing acid content, $I(0)$ is also expected to be a decreasing function. Moreover, if we take into account the related reduction in the sol concentration, $I(0)$ should exhibit a stronger decrease. For the sols we studied, an opposite behavior was observed. Consequently, we have concluded that sulfuric acid actually binds to the colloidal clusters so that its addition does not significantly modify the electron density of the solvent.

We note in Figure 2 that all the experimental points lie approximately on the same curve. This suggests that a single and well-defined function relates the mass and the radius of gyration of the aggregates for all the studied sols. Moreover, two different sets of sols containing either small ($R_g < 2.0$ nm) or large ($R_g > 2.0$ nm) aggregates can be identified because their respective experimental points lie on straight lines with different slopes. This implies that the mass and the radius of gyration of the colloidal aggregates are related by a power law (eq 5a) with clearly different exponents, this effect probably being related to differences in the mechanism of growth. We will discuss this issue in more detail later.
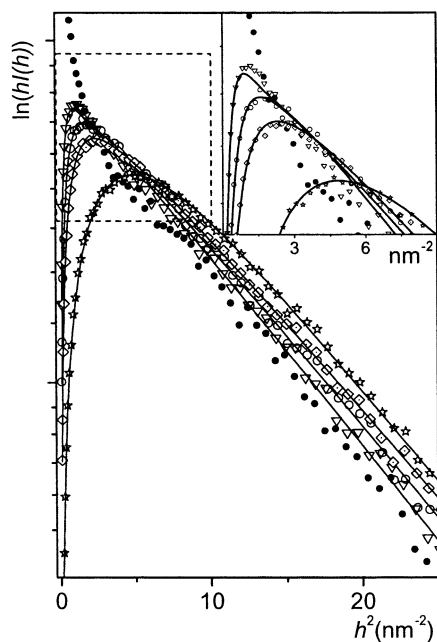
Figure 3. $\ln(hI(h))$ vs h^2 plots of the SAXS intensities corresponding to the samples listed in the second line of Table 1a. The continuous curve corresponds to the fits obtained with eqs 3 and eq 4. ●: $N = 50$; $R_o = 0.47$ nm. ▽: $N = 68$; $R_o = 0.46$ nm; $L = 5.4$ nm. ○: $N = 74$; $R_o = 0.45$ nm; $L = 3.8$ nm. ◇: $N = 80$; $R_o = 0.46$ nm; $L = 2.8$ nm. ☆: $N = 100$; $R_o = 0.47$ nm; $L = 1.4$ nm.

The experimental points for the $I(0)$ values corresponding to sols with a very high H_2SO_4 content (32 wt %) (star symbols in Figure 2) lie above the others on a slightly different and parallel straight line. The aggregates in these sols do have, in fact, a similar but not identical composition. It as been reported in the literature[44] that $[H_nSO_4]^{(2-n)-}$ sulfates can displace OH groups from hydrolyzed Zr^{IV} species and form sulfate bridges between zirconium atoms. Furthermore, zirconium sulfates have been described as structures in which the $(SO_4)^{2-}$ groups behave as bridging ligands between zirconium atoms. Consequently, the aggregates of these systems are expected to be constituted of monomers with both a different average volume and a different electronic density, as discussed in the next paragraph, thus justifying the higher $I(0)$ values.

4.1.1. Clusters (Small Aggregates). We start by focusing on the set of sols containing small colloidal particles or clusters with radii of gyration $R_g < 2.0$ nm. These clusters correspond to the experimental points lying on the straight line with lower slope in the plot displayed in Figure 2. For this set of sols the exponent D of eq 5 is equal to 0.98 ± 0.06, which is very close to 1.0. This indicates a linear dependence of mass on the radius of gyration, so suggesting that the particles are acicular or rod shaped. This result is consistent with earlier researches on analogous systems with different compositions and/or precursors.[11–16] In those studies, the presence of rod-like particles with a well-defined cross section but different lengths was also observed.

We look for another independent evidence for the rod-like shape of the clusters by analyzing the $\ln[hI(h)]$ vs h^2 plots (eq 2) of the scattered intensity. The SAXS intensities corresponding to the samples of the second line of Table 1a are plotted in Figure 3. The shape of the curves ($N = 68$ to $N = 100$) is characteristic of rod-like particles. The same shape is characteristic of all the scattering curves corresponding to the sols of the first sample set in Figure 2 (clusters with $R_g < 2.0$ nm). On the contrary, the SAXS intensity labeled $N = 50$ in
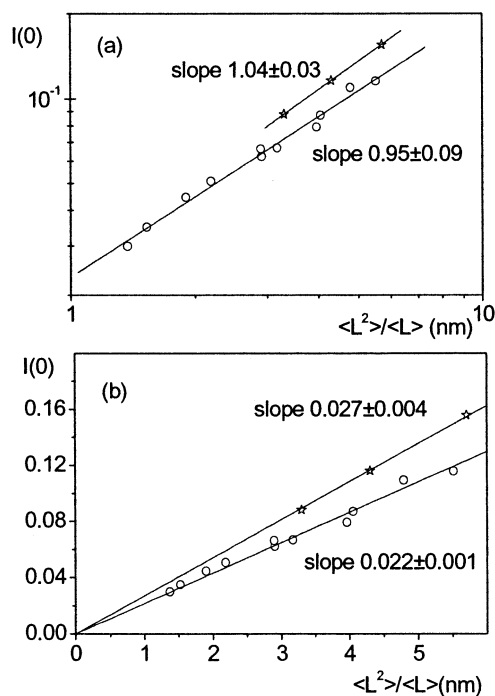
Figure 4. (a) Power-law relationship between $I(0)$ and $\langle L^2 \rangle/\langle L \rangle$ with an exponent close to 1. (b) $I(0)$ vs $\langle L^2 \rangle/\langle L \rangle$ confirms the linear dependence of the particle mass on $[\langle L^2 \rangle/\langle L \rangle]$. In both figures circles correspond to samples with $S = 8$ and stars to $S = 32$.

Figure 3, corresponding in Figure 2 to point (c) on the second straight line section, exhibits a very different shape at low h values, indicating the presence, in this case, of large and nonacicular aggregates.

The analysis of the SAXS intensities labeled $N = 68$ to $N = 100$ was performed by a fitting procedure based on eqs 3 and 4 that assume the rod-like particles to be cylindrical. Continuous lines in Figure 3 are the best-obtained fits. The radius of the clusters corresponding to the sol with $N = 50$ was evaluated from the slope of the linear region of the plots presented in Figure 3 by using eq 2. The refined radii R_o and the average lengths $\langle L \rangle$ are reported in the caption of the same figure. These results indicate that all cylinders have essentially the same radius, $R_o = 0.46 \pm 0.01$ nm, which is close to the values reported in the literature for analogous systems.[11,13] The good fits of the theoretical function given by eq 3 to all of the experimental SAXS spectra of sols containing clusters with $R_g < 2.0$ nm support the hypothesis that the small clusters have a rod-like (cylindrical) shape as those previously observed in aqueous solutions of zirconyl chloride.[14]

We can also perform an independent verification of the linear dependence of the mass of the clusters on their length. According to the description given in the Appendix, for linear growth the equation $I(0) \propto \langle L^2 \rangle/\langle L \rangle = \langle L \rangle(z + 2)/(z + 1)$ should be verified. The results plotted in Figure 4 demonstrate that the expected linear relation between $I(0)$ and $\langle L^2 \rangle/\langle L \rangle$ is experimentally verified. In the same figure the circles correspond to a sol with 8 wt % H_2SO_4 while the stars to a sol with 32 wt % H_2SO_4. The results plotted in Figure 4a indicate two power laws with an exponent close to 1.0, while the linear fits in Figure 4b, constrained to cross the origin, evidence the different proportionality factor relating $I(0)$ and $\langle L^2 \rangle/\langle L \rangle$.

Since the aggregation process in sols with a high H_2SO_4 content in sealed cells is quite slow, we were able to study, in this particular case, the kinetics of growth of the radius, length, and mass of the cylindrical colloidal clusters. Figure 5a shows

Mechanisms of Sulfate Zirconia Sol Aggregation

J. Phys. Chem. B, Vol. 107, No. 15, 2003 **3395**

Figure 5. (a) Time dependence of the radius of the cylinders and of the attenuation coefficient concerning the sol CN100H130S32 (solvent: 1-propanol). (b) Linear dependence of I(0)) vs $\langle L^2 \rangle / \langle L \rangle$ during the whole growth process.

the evolution of the radius of the rod-like clusters of the sol CN100H130S32 (1-propanol as solvent). The analysis of the SAXS curves for different aggregation times indicates that the radius of the particles does not vary during the growth process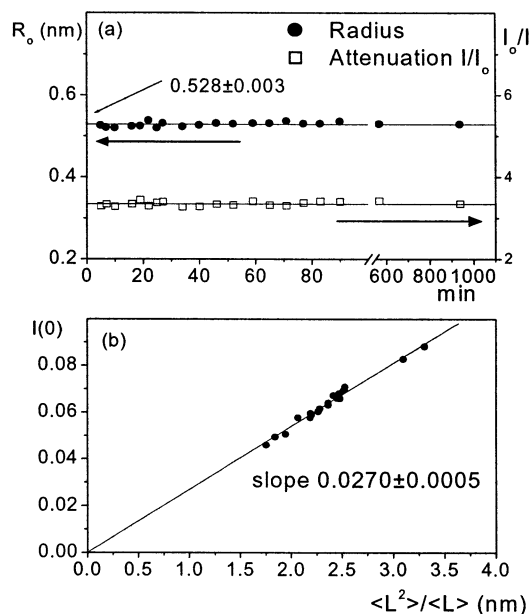 and that $I(0)$ is proportional to $\langle L^2 \rangle / \langle L \rangle$ during the entire period of evolution of the same sol (Figure 5b) with a slope $\alpha = 0.0270 \pm 0.0005$. We underline the fact that the curve plotted in Figure 4b, corresponding to three different sols with the same H_2SO_4 content at the end of the aggregation process, exhibits the same slope ($\alpha = 0.027 \pm 0.004$).

The comparison of the described results, corresponding to three sealed sols with the same H_2SO_4 content (32 wt %) at the end of their aggregation process and the kinetic evolution of one of them until its final state, suggests that the points associated to these samples, reported in Figure 2 and Figure 4b, are representative of a single growth process. In other words, each point in Figure 2 and 4b represents a frozen step of the same process of aggregation. This hypothesis will receive additional support from our study of the aggregation kinetics of open sols that will be reported later (section 4.2).

The plot $(ln[hI(h)]$ vs $h^2)$ for the sets of sols with $N = 68$ and $H = 200$ (Figure 6) and a different H_2SO_4 content (Table 1b, column 1) evidences a clear effect of sulfate content on the radius of the cylindrical clusters. The shape of the two curves with a lower H_2SO_4 content differs from the typical shape of the intensity due to rod-like particles. As already observed by previous authors,[15] the small bump in the low h region reveals the beginning of a different aggregation process and explains the position of the respective experimental points in Figure 2 (a: $H_2SO_4 = 2.0$ wt % and b: $H_2SO_4 = 0.0$ wt %) that lie on the straight line with higher slope. The radii of the cylindrical clusters, evaluated from the slope of the linear region of the plot in Figure 6 for different sulfate contents, are reported in Figure 7. We also observed that the nature of the solvent does not affect the radius of the clusters while it has an important role in the control of their length, as can be seen in Figure 8.

All of the above-reported results and the dependence of $I(0)$ on $\langle L^2 \rangle / \langle L \rangle$ indicate that sulfates are actually structurally bonded to the monomer units and that they induce right from the very
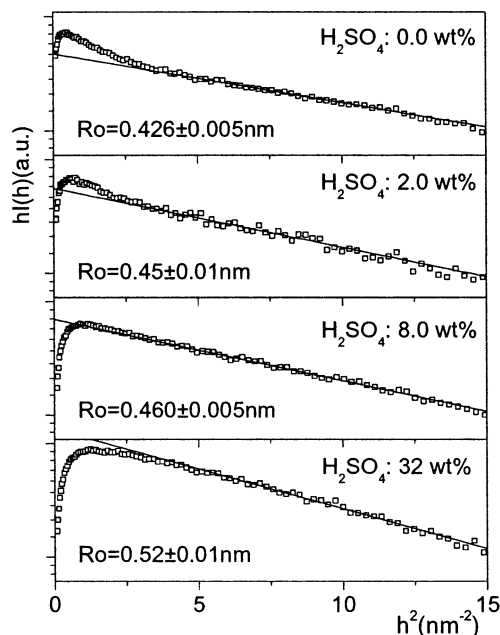
Figure 6. ln(hI(h)) vs h^2 corresponding to samples with $N = 68$, $H = 200$, and S varying from 0 up to 32 (first column of Table 1b). The radii, R_o, of the cylindrical particles are obtained from the slope of the linear portion of the curves [eq 2].
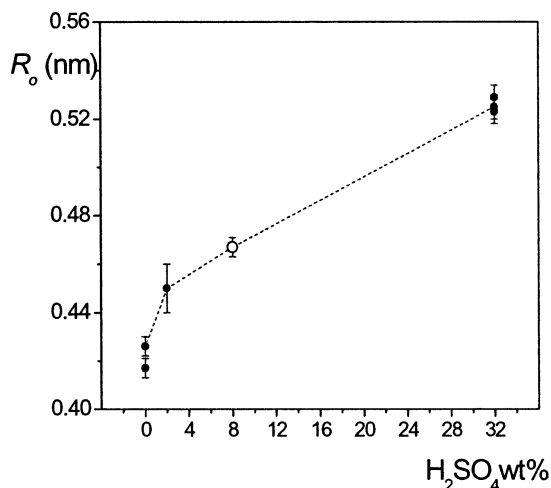
Figure 7. Effect of the H_2SO_4 content on the cylinder radius. The point corresponding to $S = 8$ (open symbol) is the average value of a large number of samples. The other points correspond to single measurements of sols with a different content of H_2SO_4.

beginning of the aggregation process a structurally different aggregate. This conclusion receives additional support from another independent argument. Since the slopes C reported in Figure 4 are proportional to $\Delta\rho^2 R^4$ (Appendix), assuming that the solvents of all sols have the same electron density, we can determine, in arbitrary units, the average electron density of the particles because we know the radii of the clusters. Our calculation yields $\Delta\rho$ values of 2.15 ± 0.05 and 1.86 ± 0.02 for sols with 8 wt % and 32 wt % H_2SO_4, respectively.

This result agrees with the hypothesis telling that the chemical composition of the cylindrical particles depends on the H_2SO_4 content. As expected, the electron density of the colloidal clusters is lower for a higher sulfate concentration, i.e., when a larger number of $[H_nSO_4]^{(2-n)-}$ groups displace OH radicals from hydrolyzed Zr^{IV} species forming $(SO_4)^{2-}$ bridges between zirconium atoms.
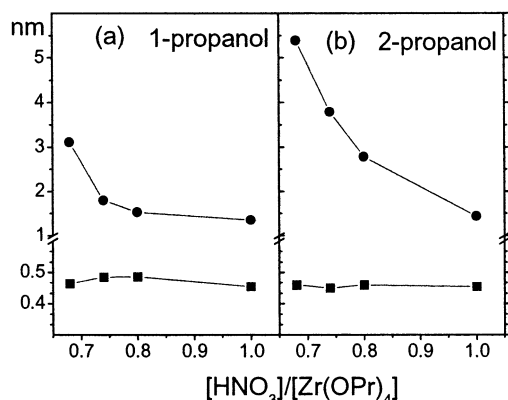
Figure 8. Dependence of the radius (squares) and the length (circles) of the cylinders on the nature of the solvent and on the HNO$_3$ content.

It is worth remarking that the results discussed in this paragraph are not biased by the particular choice of the length distribution (Shultz function). As a matter of fact, we have verified that the general conclusions of this paragraph are exactly the same (within the evaluated errors) if we use a log-normal distribution of cylinder lengths, even if, in this case, we systematically have rather worse goodness of fits.

4.1.2. Large Aggregates. As previously stated, for large aggregates ($R_g > 2.0$ nm in Figure 2), the exponent of eq 5 is $D = 1.78 \pm 0.06$. On the other hand, as was mentioned, the SAXS intensity curves plotted in Figure 6 for increasing aggregate sizes progressively deviate, at low h, from those expected for cylindrical colloidal objects. Namely, the SAXS intensities plotted in Figure 6, corresponding to the points labeled (a) and (b) of Figure 2, exhibit a small bump in the low h range. As the radius of gyration increases, the SAXS curve becomes similar to that labeled $N = 50$ in Figure 3 (point (c) in Figure 2).

The exponent $D = 1.78 \pm 0.06$ observed for $R_g > 2.0$ nm corresponds to the fractal dimension D of objects growing by the mechanism of diffusion-limited cluster aggregation (DLCA) in a three-dimensional space. Sander reported a value of $D = 1.75$,[33] meanwhile Lach-Hab et al.[45−47] calculated a value of $D = 1.80 \pm 0.01$ for dilute systems. This value was obtained by studying the radial distribution functions of simulated clusters in the flocculation regime before the gel is formed. A value $D = 1.80$ was also obtained by the same authors[47] analyzing, as in our case, the relationship between the mass M and the radius of gyration R_g for clusters submitted to a DLCA simulated experiment.

For most of the studied sols, eq 6 could not be applied because the SAXS intensity curves do not exhibit any significant linear trend in the $\text{Log}[I(h)] - \text{Log}[h]$ plot. However, we should stress that, for many of the sols studied here, the fractal dimensions obtained, when possible, by using the $\text{Log}[I(h)] - \text{Log}[h]$ plots (eq 6) do not correspond exactly to those obtained from $\log[I(0)]$ vs $\log[R_g]$ plots. This occurs because the aggregates are still small so the linear portion of $\log[I(h)] - \text{Log}[h]$ plot is limited. In fact, the scattering intensity curves of only a few of our samples exhibit a relatively well developed linear portion in the $\text{Log}[I(h)] - \text{Log}[h]$ plot (but always less than one decade in h). In these cases, the analysis yields D values slightly larger than 1.78. This difference was assigned to a contribution to the scattering intensity from the nearest-neighbor cluster region.[45]

4.2. Sols in an Open Cell. The experimental SAXS curves corresponding to the open sol (sample OBN64H400S8) prepared with the two-step method (B) are plotted in Figure 9. These results indicate a smooth evolution of the structure (fast or slow
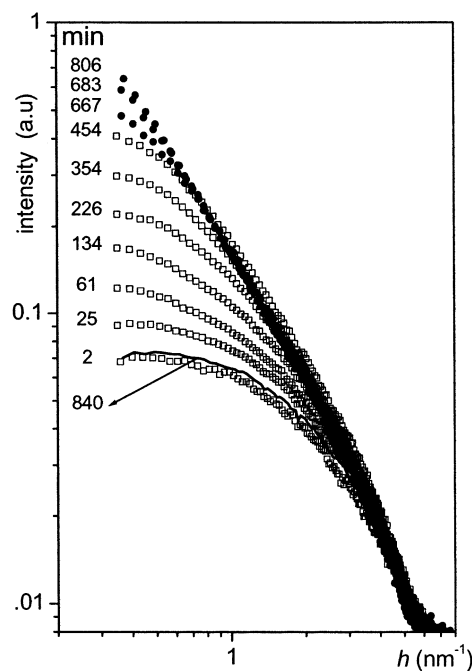

Figure 9. Time-resolved measurements of the scattering intensity of the sample OBN64H400S8 in an open cell. The empty and filled symbols correspond, respectively, to SAXS intensities before and after water addition. The curve (continuous line) corresponds to the same sample, before water addition, and kept for 840 min in a sealed cell.

depending on the chemical conditions) starting even before the addition of the amount of water necessary to promote the hydrolysis process. This evolution occurs because the solution absorbs water needed for the hydrolysis reaction from the atmosphere. We can exclude that this effect is promoted exclusively by the small amount of water present in the acids; in fact the structure of the same sol inside a sealed cell, even after several hours, did not exhibit any significant structure variation. Since the absorption of water is very slow, the growth of the aggregates is a very slow process, thus allowing for time-resolved SAXS measurements to be performed.

We have also observed a progressive increase in the attenuation factor defined by I_0/I_T, where I_0 is the intensity of the primary beam and I_T the same intensity attenuated by the sample. The variation of the attenuation factor indicates that the concentration of the open sols progressively increases. This ratio does not vary when the measurements are performed using sealed cells (Figure 5a). It is worth mentioning that the attenuation factor, I_0/I_T, strongly depends on the solvent concentration but it is almost independent of water and/or HNO$_3$ content. This increasing sol concentration may also be responsible for the different behavior observed for sealed and open systems.

Concerning the same SAXS measurements associated to open sols OBN64H400S8, we noticed that the $\ln(hI(h))$ vs h^2 plots (Figure 10) are very similar to those reported by Hu et al.[15] and to our results corresponding to sealed samples (Figure 3 and Figure 6).

It is noteworthy to stress that the scattering curves corresponding to intermediate stages of the growth process in open sols are equivalent to those associated to final states of samples in a sealed cell under specific preparation conditions. In fact, during the first stages of aggregation in open cell, the SAXS intensity curves have the shape expected for rod-like particles. At more advanced stages of aggregation, the SAXS curves progressively change their shape.
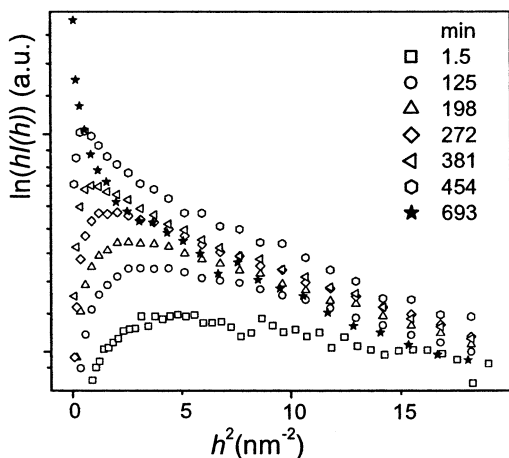
Mechanisms of Sulfate Zirconia Sol Aggregation

J. Phys. Chem. B, Vol. 107, No. 15, 2003 **3397**

Figure 10. $\ln(hI(h))$ vs h^2 plots for the sample OBN64H400S8 at different stages of aggregation. Water was added at $t = 660$ min.
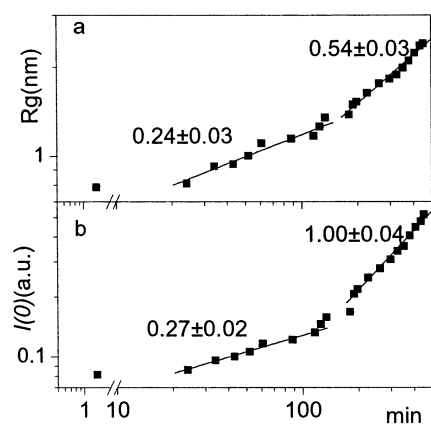

Figure 11. Time variation of the radius of gyration R_g and $I(0)$ (proportional to the aggregate mass) for sample OBN64H400S8 before water addition. The slopes are indicated in the figure.

Before the addition of water, the system OBN64H400S8 passes from a first stage of aggregation, when acicular (cylindrical) small clusters grow, to a second stage corresponding to the formation of large aggregates. This can clearly be seen in the $I(0)$ and R_g vs time (t) plots corresponding to the same sol (OBN64H400S8) in an open cell (Figure 11) before the addition of water. The radius of gyration R_g and $I(0)$, and thus the mass M, exhibit a power time dependence after the first minutes of growth ($I(0) \propto t^\alpha$ and $R_g \propto t^\beta$). This type of power dependence was also determined by computer simulation of DLCA processes.[46] This implies that $I(0) \propto R_g^{\alpha/\beta}$. From the values of the slopes α and β determined from our experimental results (Figure 11), we have obtained the quotient $\alpha/\beta = 1.12 \pm 0.03$ for the early aggregation stage, this value being close to 1, as expected for 1-D growth. The quotient $D = \alpha/\beta$ is equal to 1.9 ± 0.1 for advanced stages of aggregation. This D value is close to that expected for the mechanism of DLCA, in agreement with the characteristic exponent determined using the final equilibrium data of sols in closed cells. We can also observe that, during the advanced stage of aggregation, the intensity $I(0) \propto \langle k^2 \rangle / \langle k \rangle \propto t^\alpha$ with an exponent $\alpha = 1.00 \pm 0.04$ which is equal, within the experimental error, to the value 1.07 ± 0.06 obtained from computer simulation calculations.[46]

5. Summary and Conclusions

In Figure 12 we have plotted together the $\log[I(0)]$ vs $\log[R_g]$ functions corresponding to all sol compositions analyzed during aggregation process in open cells and the final states in sealed
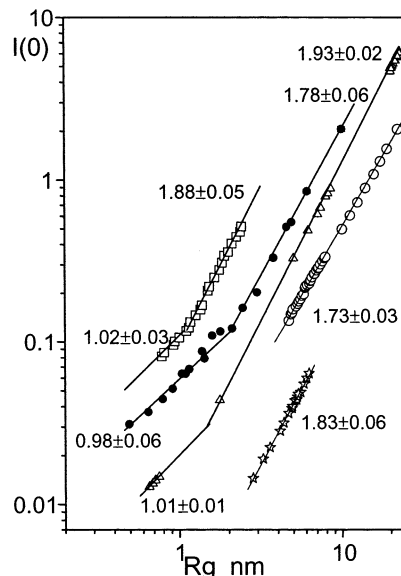

Figure 12. Plots of $\text{Log}(I(0))$ vs $\text{Log}(R_g)$ for different samples. The observed linear dependences indicate that $I(0) (\propto M) \propto R_g^D$. The slopes D are reported in the plot. While the filled symbols correspond to the data reported in Figure 2 (final states of the samples in closed cells), the open symbols are kinetic data of samples in open cells. The curves corresponding to the open samples were vertically displaced for clarity. ●: Closed systems. ○: ON80H400S8. △: OBN90H400S0 (H_2O added after 10 min). ☆: OBN100H400S0 (after H_2O addition). □: OBN64H400S8 (before H_2O addition).

cells. This plot once again indicates the presence of two well-defined mechanisms for the growth of aggregates that appear to be the same for the whole series of studied sols. In the early stages, the main process is the growth of acicular (cylindrical) clusters of progressively increasing length and constant cross-section. The aggregation of these clusters later builds up large nonlinear aggregates.

The slight difference in the exponent of the $I(0)$ vs R_g function observed for the sols in an open cell may be due to the mentioned small increasing concentration of the sol and/or to small fluctuation of the thickness of the sample produced by the somewhat flexible Mylar windows. Nevertheless, we can conclude that two well-defined mechanisms characterize the growth either in sealed or in open cells. In the open cells, the transition between the two growth regimes takes place for a radius of gyration of 1.3–1.4 nm, close to previous results ($R_g = 1.5$ nm) obtained by Chaumont et al.[11] This value is slightly smaller than the value $R_g = 2.0$ nm that we have determined for sealed cells.

Concerning the general mechanism of the aggregation process and structure variations, previous investigations[11,12,14] proposed that polymer random coils are formed because the fractal dimension D was found to vary in the range $D = 1.67-2.00$. These values, similar to those determined in this study, are characteristic of coils with excluded volume in a good solvent. Another fact supporting this model is the existence of a linear portion in the $\text{Log}[I(h)]$ vs $\text{Log}[h]$ plot with slope close to 1 that may be associated with the persistence length of quite rigid polymers.[11,12] Moreover, the previous investigations recognized the difficulty of distinguishing this model from that of a disordered association of needle-like colloidal objects leading to large aggregates probably held together by hydrogen bonds between OH groups on adjoining chains.[11,14]

Even if we cannot establish a definitive conclusion, we believe that the mechanism of formation of needle-like clusters followed by their subsequent aggregation is more consistent with

our experimental results. As a matter of fact, our results indicate that two clearly different mechanisms dominate the growth in two subsequent and well-defined time periods. On the contrary, in the polymeric (random) coil model, the linear objects would become progressively longer and more flexible, and so a well-defined transition to a second regime is not a priori expected. Finally, we should mention that the sols that we investigated are still in the flocculation regime (before the sol−gel transition) so we cannot assign the observed sharp variation in the rate of mass growth to a sudden change in viscosity.

Appendix

A1. Derivation of Equation 5a for a Set of Aggregates with a Size Distribution. The SAXS intensity produced by a dilute set of colloidal objects can be written as follows:[17]

$$I(h) = I_e(h)N\sum_k p_k\langle F_k^2\rangle \cong K_oN\sum_k p_k\langle F_k^2\rangle \quad (A1)$$

where $I_e(h) = 7.9 \times 10^{-26}I_o\,d^{-2} \times (1 - \cos^2(2\theta))/2$ (I_o being the intensity of the incident beam and d the sample-to-detector distance), N is the number of colloidal particles in the irradiated volume, p_k is the probability that one of the particles is of type k, $\langle F_k^2\rangle = V_k^2\Delta\rho_k^2 i_k(h)$ is the form factor of the particle k averaged for all possible orientations (V_k being the volume of particle k, $\Delta\rho_k$ the difference between the electron densities of the particles and of the matrix (solvent), and $i_k(h)$ a function depending on the particle shape with $i_k(0) = 1$). $I_e(h)$ is usually approximated by a constant value K_o within the small h range.

If the particles are built up by progressive aggregation of monomers, we can assume that $p_k = P(k)$, $P(k)$ being the probability that a particle be composed of k monomers, and $\langle F_k^2\rangle$ is the form factor of an aggregate of k monomers. In this case $\Delta\rho_k = \Delta\rho$ is the same for all the clusters and $V_k = kv_o$, v_o being the volume of the monomer.

Assuming that the total number of monomers, m, in the irradiated sample is constant during the cluster growth, we have $N = m/\langle k\rangle$, where $\langle k^n\rangle$ is the nth moment of the number of monomers or mass distribution. Under these assumptions the intensity becomes

$$I(h) \cong K_o v_o^2\Delta\rho^2\frac{m}{\langle k\rangle}\sum_k p_k k^2 i_k(h) \quad (A2)$$

with $I(0) = K_o v_o^2\Delta\rho^2(\langle k^2\rangle/\langle k\rangle)m$. Since the mass of the aggregates is proportional to k, the intensity $I(0)$ is proportional to ratio of the second and the first moments of mass distribution.

In the low h range we can use the Guinier approximation of the intensity (eq A2), so obtaining the average value of the radius of gyration:

$$I(h) \cong K_o v_o^2\Delta\rho^2\frac{m\langle k^2\rangle}{\langle k\rangle}\sum_k p_k\frac{k^2}{\langle k^2\rangle}\left(1 - \frac{R_{gk}^2 h^3}{3} + O(h^4)\right)$$

$$= K_o v_o^2\Delta\rho^2\frac{m\langle k^2\rangle}{\langle k\rangle}\left(1 - \frac{\overline{R_g^2}h^3}{3} + O(h^4)\right) \quad (A3)$$

where R_{gk}^2 and $\overline{R_{gk}^2}$ are respectively the squared radius of gyration of the aggregate of k monomers and the average

squared radius of gyration of the collection of aggregates. Since in general the mass of the aggregates (proportional to k) is related to the radius of gyration by a power law, we can write $k \propto R_{gk}^D$ so

$$\overline{R_g^2} = \sum_k \frac{p_k}{\langle k^2\rangle}k^2 R_{gk}^2 = \frac{\langle R_g^{2D+2}\rangle}{\langle R_g^{2D}\rangle} \quad (A4)$$

The average radius of gyration that is experimentally determined using Guinier or Zimm plots is then given by

$$\overline{R_g} = \left(\overline{R_g^2}\right)^{1/2} \quad (A4a)$$

When all the aggregates are constituted of the same number of monomers $I(0) \propto k \propto R_{gk}^D$, but in general this relation does not hold for an arbitrary distribution p_k.

It is known that in colloidal particle aggregation the aggregate mass distribution undergoes a dynamic scaling.[45−48] As verified by many authors, the number $N(k,t)$ of aggregates constituted of k monomers at the time t during the aggregation process is

$$N(k,t) = Np_k \cong \frac{m}{\langle k(t)\rangle^2}f\left(\frac{k}{\langle k(t)\rangle}\right) \cong \frac{m}{\langle k(t)\rangle_w^2}f'\left(\frac{k}{\langle k(t)\rangle_w}\right) \quad (A5)$$

where $\langle k(t)\rangle$ is the average number of monomers constituting the aggregates at time t and $\langle k(t)\rangle_w = \langle k^2(t)\rangle/\langle k(t)\rangle$ and $f(x), f'(x)$ are universal functions displaying an asymmetrical bell shape in the low concentration limit. It is easy to prove that $\int_0^\infty f(x)\,dx = \int_0^\infty xf(x)\,dx = 1$. In DLCA and in low concentration limit $\langle k(t)\rangle \cong t^z$ and $\langle k(t)\rangle_w \cong t^{z1}$ with $z \cong z1 \cong 1$.

Taking into account that $k \propto R_{gk}^D$, we can obtain the normalized gyration radii distribution:

$$P(R_g,t) = \frac{DR_g^{D-1}}{\langle R_g^D(t)\rangle}f\left(\frac{R_g^D}{\langle R_g^D(t)\rangle}\right) \quad (A6)$$

The scaling properties of this distribution imply that

$$\langle R_g^n\rangle = \langle R_g^D\rangle^{n/D}\int_0^\infty x^{n/D}f(x)\,dx \equiv \alpha(n/D)\langle R_g^D\rangle^{n/D} \quad (A7)$$

Because of this notable property, we conclude that

$$I(0) \propto \frac{\langle k^2\rangle}{\langle k\rangle} \propto \frac{\langle R_g^{2D}\rangle}{\langle R_g^D\rangle} = \alpha(2)\langle R_g^D\rangle \quad (A7a)$$

On the other side the measured radius of gyration

$$\overline{R_g^2} = \frac{\langle R_g^{2D+2}\rangle}{\langle R_g^{2D}\rangle} = \frac{\alpha(2 + 2/D)}{\alpha(2)}\langle R_g^D\rangle^{2/D} \quad (A7b)$$

Because of the universality of the function $f(x)$ in the aggregation process of colloidal particles:

$$I(0) \propto \left(\overline{R_g^2}\right)^{D/2} \quad (A8)$$

and, as specified in eq 5a, the average radius of gyration experimentally measured, $\overline{R_g} = \left(\overline{R_g^2}\right)^{1/2}$ becomes

$$I(0) \propto \overline{R_g}^D \quad (A9)$$

Mechanisms of Sulfate Zirconia Sol Aggregation

J. Phys. Chem. B, Vol. 107, No. 15, 2003 **3399**

A2. Derivation of Equation 3 for a Set of Cylindrical Objects with a Length Distribution. If all the particles are cylinders with the same radius R and variable heights L, with a probability distribution $P(L)$, we can assume the monomers to be a cylinder with length L_o and R constant. In this case $v_o = \pi R^2 L_o$ and[17]

$$i(L,h) = \int_0^{\pi/2} \frac{\sin^2(hL\cos\vartheta/2)}{(hL\cos\vartheta/2)^2} \frac{4J_1^2(hR\sin\vartheta)}{(hR\sin\vartheta)^2} \sin\vartheta \, d\vartheta \quad (A10)$$

where J_1 is the first-order Bessel function.

Finally the scattered intensity becomes

$$I(h) = K_o(\pi R^2 L_o)^2 \Delta\rho^2 \frac{m}{\langle L \rangle} \int_0^\infty P(L)L^2 i(L,h) =$$

$$\frac{I(0)}{\langle L^2 \rangle} \int_0^\infty P(L)L^2 i(L,h) \quad (A11)$$

with $I(0) = K_o(\pi R^2 L_o)^2 \Delta\rho^2(\langle L^2 \rangle/\langle L \rangle) \equiv C(\langle L^2 \rangle/\langle L \rangle)$, where the constant C is proportional to $\Delta\rho^2 R^4$.

We have assumed that the heights of the cylinders follow a Shultz distribution:

$$P(L) = \frac{1}{\Gamma(z+1)}\left(\frac{z+1}{\langle L \rangle}\right)^{z+1} L^z \, e^{[-(z+1)L/\langle L \rangle]} \quad (A12)$$

with $z > -1$ and

$$\langle L^n \rangle = \frac{(z+1)(z+2)...(z+n)}{(z+n)^n}\langle L \rangle^n$$

The parameter z controls the shape of the distribution that approximates the Dirac function $\delta(L - \langle L \rangle)$ when $z \to \infty$. The distribution is rightward-skewed and has a maximum at $L = z\langle L \rangle/(z+1)$ when $z > 0$; if $z = 0$ it is a decreasing exponential function, and finally if $-1 < z < 0$ it diverges at $x = 0$.

The expression of the SAXS intensity $I(h)$ requires (as specified in eq 3) the evaluation of two integrals:

$$I(h) = \frac{I(0)}{\langle L^2 \rangle}\int_0^{\pi/2} \frac{4J_1^2(hR\sin\vartheta)}{(hR\sin\vartheta)^2}\sin\vartheta \, d\vartheta \int_0^\infty P(L)L^2 \times$$

$$\frac{\sin^2(hL\cos\vartheta/2)}{(hL\cos\vartheta/2)^2} \, dL \quad (A13)$$

For a $P(L)$ function described by the Schultz distribution (eq A12), the second integral can be analytically evaluated yielding

$$\int_0^\infty P(L)L^2 \frac{\sin^2(hL\cos\vartheta/2)}{(hL\cos\vartheta/2)^2} \, dL = \frac{1}{2h^2\cos^2(\theta)} \times$$

$$\left\{1 - \left[\frac{1}{1+x^2}\right]^{[(z+1)/2]}\cos[(z+1)\tan^{-1}(x)]\right\} \quad (A14)$$

where

$$x = \frac{2h\langle L \rangle \cos(\theta)}{(z+1)}$$

References and Notes

(1) Ward, D. A.; Ko, E. I. *Chem. Mater.* **1993**, *5*, 956−969.
(2) Kozuka, H.; Kuroki, H.; Sakka, S. *J. Non-Cryst. Solids* **1988**, *100*, 226−230.
(3) Sanchez, C.; Livage, J.; Henry, M.; Babonneau, F. *J. Non-Cryst. Solids* **1988**, *100*, 65, 76.
(4) Tanabe, K.; Yamaguchi, T. *Stud. Surf. Sci. Catal.* **1989**, *44*, 99−110.
(5) Davis, B. H.; Keogh, R. A.; Srinivasan, R. *Catal. Today* **1994**, *20*, 219−256.
(6) Song, X.; Sayari, A. *Catal. Rev. Sci. Eng.* **1996**, *38*, 329−412.
(7) Corma, A. *Chem. Rev.* **1995**, *95*, 559−614.
(8) Arata, K. *Adv. Catal.* **1990**, *37*, 165−212.
(9) Hino, M.; Arata, K. *J. Chem. Soc., Chem. Commun.* **1980**, *18*, 851−852.
(10) Minesso, A.; Genna, F.; Finotto, T.; Baldan, A.; Benedetti, A. *J. Sol−Gel Sci. Technol.* **2002**, *24*, 197−207.
(11) Chaumont, D.; Craievich, A.; Zarzycki, J. *J. Non-Cryst. Solids* **1992**, *147&148*, 127−134 and references therein.
(12) Singhal, A.; Beaucage, G.; Harris, M. T.; Toth, L. M.; Keefer, K. D.; Lin, J. S.; Hu, M. Z.-C.; Peterson, J. R. *J. Non-Cryst. Solids* **1999**, *246*, 197−208.
(13) Toth, L. M.; Lin, J. S.; Felker, L. K. *J. Phys. Chem.* **1991**, *95*, 3106−3108.
(14) Jutson, J. A.; Richardson, R. M.; Jones, S. L.; Noman, C. *Mater. Res. Soc. Symp. Proc.* **1990**, *180*, 123−128.
(15) Hu, M. Z.-C.; Zielke, J. T.; Lin, J. S.; Byers, C. H. *J. Mater. Res.* **1999**, *14*, 103−113.
(16) Singhal, A.; Toth, L. M.; Lin, J. S.; Affholter, K. *J. Am. Chem. Soc.* **1996**, *118*, 11529−11534.
(17) Guinier, A.; Fournet, G. *Small Angle Scattering of X-rays*; Wiley: New York, 1955.
(18) Porod, G. In *Small Angle X-ray Scattering*; Glatter, O, Kratky, O., Eds.; Academic Press: London, 1982.
(19) Schultz, G. V. Z. *Physik. Chem.* **1939**, *B44*, 227−247.
(20) Zimm, B. H. *J. Chem. Phys.* **1948**, *16* 1093−1099 and 1099−1116.
(21) Boyd, R. H.; Phillips P. J. *The science of polymer molecules*; Cambridge University Press: Cambridge, 1993.
(22) Feigin, L. A.; Svergun, D. I. *Structure Analysis by Small-Angle X-ray and Neutron Scattering*; Plenum Press: New York, 1987.
(23) Mandelbrot, B. B. *Fractal Form, Chance and Dimension*; Freeman: San Francisco, 1977, or *Les objects fractals, forme, hasards et dimension*, 3rd ed.; Nouvelle bibliothèque scientifique: Flammarion, 1989.
(24) Jullien, R.; Botet, R. *Aggregation and Fractal Aggregates*; World Scientific: Singapore, 1987.
(25) Schaefer, D. W.; Martinm J. E. *Phys. Rev. Lett.* **1984**, *52*, 2371−2374.
(26) Wijnen, P. W. J. G.; Beelen, T. P. M.; Rummens, K. P. J.; Saeijs, H. C. P. L.; De Haan, J. W.; van De Ven, L. J. M.; van Santen, R. A. *J. Colloid Interface Sci.* **1991**, *145*, 17−32.
(27) Meakin, P. *Phase Trans. Crit. Phenom.* **1988**, *12*, 335−489.
(28) Aubert, C.; Cannel, D. S. *Phys. Rev. Lett.* **1986**, *56*, 738−741.
(29) Beelen, T. P. M.; Dokter, W. H.; Van Garderen, H. F.; Van Santen, R. A. *Adv. Colloid Interface Sci.* **1994**, *50*, 23−37.
(30) Cabane, B.; Dubois, M.; Lefaucheux, F.; Robert, M. C. *J. Non-Cryst. Solids* **1990**, *119*, 121, 131.
(31) Dokter, W. H.; Beelen, T. P. M.; van Garderen, H. F., Van Santen, R. A. *Mater. Res. Soc. Symp. Proc.* **1994**, *346* (Better Ceramics Through Chemistry), 217−222.
(32) Krakovsky, I.; Urakawa, H.; Kajiwara, K.; Kohjiya, S. *J. Non-Cryst. Solids* **1998**, *231*, 31−40.
(33) Sander, L. M. *Contemp. Phys.* **2000**, *41*, 203−218.
(34) Radlinski, A. P.; Radlinska, E. Z.; Agamalian, M.; Wignall, G. D.; Lindner, P.; Randl, O. G. *Phys. Rev. Lett.* **1999**, *82*, 3078, 3081.
(35) Schmidt, P. W. In *The Fractal Approach to Heterogeneous Chemistry: Surfaces, Colloids, Polymers*; Avnir, D., Ed.; Wiley: Singapore, 1989.
(36) Avnir, D.; Biham, O.; Lidar, D.; Malcai, O. *Science* **1998**, *279*, 39−40; see also the related letters by Mandelbrot, B. B.; Pfeifer, P. *Science* **1998**, *279* 783−784 and Tsonis, A. A. *Science* **1998**, *279*, 1611 and the answer by Biham, O.; Malcai, O.; Lidar, D.; Avnir, D. *Science* **1998**, *279*, 783−784 and 1611.
(37) Wen Li, W.; Bauer, L. B. J.; Su, W. *Polymer* **1989**, *30*, 1384−1388.
(38) Suh, D. J.; Park, T. J. *Chem. Mater.* **1996**, *8*, 509−513.
(39) Stöcker, C.; Baiker, A. *J. Non-Cryst. Solids* **1998**, *223*, 165−178.
(40) Ward, D. A.; Ko, E. I. *Chem. Mater.* **1993**, *5*, 956−969.
(41) Ward, D. A.; Ko, E. I. *J. Catal.* **1994**, *150*, 18−33.
(42) Bedilo, A. F.; Klabunde, K. J. *J. Catal.* **1998**, *176*, 448−458.
(43) Cavalcanti, L. P.; Kellermann, G.; Plivelic, T.; Neuenschwander, R.; ITorriani LNLS Activity Report, 2000, 5−6.
(44) Livage L. *Catal. Today* **1998**, *41*, 3−19.
(45) Lach-Hab, M.; González, A. E.; Blaistein-Barojas, E. *Phys. Rev. E* **1998**, *57*, 4520−4527.
(46) Lach-Hab, M.; González, A. E.; Blaistein-Barojas, E. *Phys. Rev. E* **1996**, *54*, 5456−5462.
(47) González, A. E.; Lach-Hab, M.; Blaistein-Barojas, E. *J. Sol−Gel Sci. Technol.* **1999**, *15*, 119−127.
(48) Van Dongen, P. G. J.; Ernst, M. H. *Phys. Rev. Lett.* **1985**, *54*, 1396−1399.